Shrewd Sine–Cosine Algorithm Based Double Integral Tilt Derivative Controller for Frequency Regulation of Multi Microgrid System

--Manuscript Draft--

Manuscript Number:	
Full Title:	Shrewd Sine–Cosine Algorithm Based Double Integral Tilt Derivative Controller for Frequency Regulation of Multi Microgrid System
Article Type:	Original research
Funding Information:	
Abstract:	The presence of renewable source uncertainties, varying loading circumstances and lack of rotating inertia makes the load frequency regulation of a microgrid (MG) system a tedious task. This necessitates a robust and intelligent frequency control strategy for stable functioning of the MG system. The research paper presents the implementation of a novel Double Integral Tilt Derivative with Filter (DITDF) controller for load Frequency regulation of a multiarea microgrid (MMG) System. An improved version of the existing Sine–Cosine Algorithm (SCA), i.e. Shrewd Sine–Cosine Algorithm (SSCA) has been purposed to optimize the parameters of the suggested DITDF controller. The validity of the SSCA is tested on a set of benchmark problems to show the enhanced efficiency of the SSCA. For real-world application of the proposed algorithm, a comparative study has been synthesized to demonstrate the potency of the proposed SSCA algorithm over Genetic Algorithm (GA), Particle Swarm Optimization (PSO) and SCA in regard to the frequency control of a MG system. For controller supremacy examination, the performance of the proposed DITDF controller is compared with conventional PID, TIDF, ITDF controllers, and it has been revealed that the proposed SSCA tuned DITDF controller exhibits better performances through the different intermittent conditions of MG analysis. Finally, sensitivity analysis is performed to illustrate the adaptability of the suggested technique to a wide range of MMG parameters. It is observed that even in the worst-case scenario considered in the manuscript; the proposed SSCA-DITDF control scheme outperformed its counterparts like PID, TIDF and ITDF controller by 38.78%, 32.12% and 18.99%.
Corresponding Author:	SATYAJEET DAS Veer Surendra Sai University of Technology INDIA
Corresponding Author E-Mail:	satyajeetburla@gmail.com
Corresponding Author Secondary Information:	
Corresponding Author's Institution:	Veer Surendra Sai University of Technology
Corresponding Author's Secondary Institution:	
First Author:	Satyajeet Das
First Author Secondary Information:	
Order of Authors:	Satyajeet Das
	Sidhartha Panda
Order of Authors Secondary Information:	
Suggested Reviewers:	
Opposed Reviewers:	
Additional Information:	
Question	**Response**
Are you submitting this manuscript to a	No

Thematic Series?	

Shrewd Sine–Cosine Algorithm Based Double Integral Tilt Derivative Controller for Frequency Regulation of Multi Microgrid System

Abstract

The presence of renewable source uncertainties, varying loading circumstances and lack of rotating inertia makes the load frequency regulation of a microgrid (MG) system a tedious task. This necessitates a robust and intelligent frequency control strategy for stable functioning of the MG system. The research paper presents the implementation of a novel Double Integral Tilt Derivative with Filter (DITDF) controller for load Frequency regulation of a multiarea microgrid (MMG) System. An improved version of the existing Sine–Cosine Algorithm (SCA), i.e. Shrewd Sine–Cosine Algorithm (SSCA) has been purposed to optimize the parameters of the suggested DITDF controller. The validity of the SSCA is tested on a set of benchmark problems to show the enhanced efficiency of the SSCA. For real-world application of the proposed algorithm, a comparative study has been synthesized to demonstrate the potency of the proposed SSCA algorithm over Genetic Algorithm (GA), Particle Swarm Optimization (PSO) and SCA in regard to the frequency control of a MG system. For controller supremacy examination, the performance of the proposed DITDF controller is compared with conventional PID, TIDF, ITDF controllers, and it has been revealed that the proposed SSCA tuned DITDF controller exhibits better performances through the different intermittent conditions of MG analysis. Finally, sensitivity analysis is performed to illustrate the adaptability of the suggested technique to a wide range of MMG parameters. It is observed that even in the worst-case scenario considered in the manuscript; the proposed SSCA-DITDF control scheme outperformed its counterparts like PID, TIDF and ITDF controller by 38.78%, 32.12% and 18.99%.

Keywords: Load Frequency control, Double Integral Tilt Derivative with Filter controller, Shrewd Sine–Cosine Algorithm, Microgrid, Electric vehicle, Ultra- Capacitor

1. Introduction

In the contemporary world, the power sector is transitioning towards the distributed power generation and distribution from the orthodox centralized power generation and distribution [1]. The liberalization of the Energy market, strict emission commitments like the Kyoto protocol, myriad environmental concerns, and soaring charges of energy transmission and distribution has further fast-tracked this trend. Microgrid (MG) is a viable option in this approach to promote the use of a mix of sustainable and conventional power sources to curtail complete dependence on conventional power sources. An MG is fundamentally composed of small generation and load units that are placed in several locations and can function in either grid-connected or standalone mode. In the case of grid-connected systems, the primary goal is to provide auxiliary services to the overhead system while also optimizing internal energy management. On the other hand, in standalone mode, it can be utilized to feed remote applications or improve the power quality of weak grids [2]. Apart from the core functionality, there are myriad other advantages of amalgamating MG into distribution systems: firstly, the distributed energy resources(DER) units present in a MG can provide for the local energy demand, hence limit its dependence on the upper-level utility grid and augments the reliability of power supply; secondly, MG facilitates environmentally-friendly energy consumption by employing renewable energy based generators, i.e., photovoltaic panels, fuel cells, and wind turbines; finally, MG can curtail long-distance transmission loss, by using local distributed generators to meet energy needs.

With the growing penetration of renewable energy in power networks, the idea of multi-microgrid (MMG) has recently emerged on the scene, which corresponds to a cluster of MGs

interconnected in close electrical or spatial proximity [3]. MMG's goal is to create greater resilience, controllability and stability by utilizing quick power exchange, as well as a high and consistent penetration of DERs into the bulk system. Moreover, MGs in MMG system can support each other when connected.

Although, the MMG system provide numerous advantages, they face some serious challenges. Due to variations in load, the presence of unanticipated uncertainties, such as in wind and PV system, conflicts with the conventional system, such as the absence of rotating inertia, the variations in the effects of line impedance on active and reactive power control, an imbalance of power between the total generation and the total demand occurs in the standalone mode operation [4]. As a result, MMG performance is insecure, particularly in terms of active power and frequency. These imbalances can result in consequences as serious as blackout. Moreover, an MMG has distinct characteristics with a more complex architecture as compared to individual MGs because energy exchange is allowed between MGs in an MMG system. Thus, the operation strategy of an MMG system is more complex than a single MG, which directly affect the performance of the MMG system [5]. This further elevates the Load Frequency Control (LFC) problem, which necessities a robust and intelligent control strategy for obtaining satisfactory performance for MMG system.

To address LFC issues, an intelligent and versatile controller is essential, one that can perform in a range of situations and ensure reliable operations [6]. Since a smooth frequency control necessitates a robust controller, several researchers have proposed various controllers using different intelligent approaches, such as fuzzy methodology [7 - 12], neural network (NN) [13 - 14], fractional-order controllers [15-17], cascading theory [15, 18]. However, most of the proposed strategies were either implemented in the MG system or traditional multi-area power

system, not in an MMG system. The concept of MMG being relatively new; as a result, its literary work in the field of LFC in MMG has been minimal. [8 - 9, 14, 17 - 18].

In recent, fractional order controller have gained popularity over years due to amelioration in adaptableness and effectiveness in controller performance and design [19]. TID is one category of fractional order controller. The Tilt-Integral-Derivative (TID) was first patented few decades back in [20], citing its improved feedback over the robust Proportional–Integral–Derivative (PID) controller. Additionally, TID compensators enabled simpler tuning, higher disturbance rejection ratios, and reduced effects of plant parameter fluctuations on closed loop response, resulting in their employment in a variety of engineering fields. However, its first application in the field of LFC was presented just a few years back in [21]. A TID with filter (TIDF) [21] controller can be obtained from the traditional PID by multiplying the proportional component of the PID with transfer function S^((-1)/n) and adding a filter component to eliminate the chattering problem of the derivative component. Recently, Researchers have started using hybrid tilt controller for the purpose of frequency regulation like control fuzzy-TIDF [22], Integral Tilt Derivative with Filter controller (ITDF) [23], etc. In this manuscript, a novel Double Integral Tilt Derivative with Filter controller (DITDF) is purposed to address the LFC problem arising in the MMG system.

As discussed above, an effective LFC requires an appropriate controller design, which necessitates proper tuning of controller parameters. To design the controller gains, a variety of methodologies have been proposed, including Genetic Algorithm (GA) [24], Particle Swarm Optimization (PSO) [10], Gravitational Search Algorithm (GSA) [25], Grey Wolf Optimizer (GWO)[26], Slap Swarm Algorithm (SSA) [27], Differential Evolution (DE) [11], Teaching Learning Based Optimization (TLBO) [16], Sine–Cosine Algorithm (SCA) [15, 28],

Equilibrium optimizer (EO)[29] and others. SCA is one of the recent and most popular algorithms [28]. In terms of exploration and exploitation, SCA has proven its worth. Because of its excellent exploring capabilities, it has been used to solve a plethora of real-world challenges like feature selection [30], load forecasting [31], LFC [15], optimal power flow problem [32], power quality conditioner allocation in the distribution system [33], healthcare [34] etc. However, the SCA, like other meta-heuristic algorithms, face the same an issue with local optima stagnation and pre-mature convergence. As a result, some modification is required to enhance its performance. The present article proposes a modified SCA, namely Shrewd Sine–Cosine Algorithm (SSCA), to overcome the drawbacks of SCA and provide results closer to the global optimum. To the best of our knowledge, the presented variant of SCA has never been discussed. The suggested algorithm's effectiveness is also compared in the manuscript with the classical SCA, popular algorithms (GA, PSO, GWO, GSA and SSA) and some recent modified versions of SCA proposed by researchers [35-40], using standard benchmark tests. The proposed SSCA is then employed in a real-world engineering problem for tuning of the parameters of the controllers. Numerous Simulation results are provided, which reveals the efficacy of the SSCA based DITDF controller to perform satisfactorily and provides better dynamic performance in contrast with other strategies for LFC of MMG. The major contribution of the proposed work is presented as below:

1. Implementation of MMG comprises of several components such as Wind Turbine Generator (WTG), Photovoltaic system (PV), Ultra Capacitor (UC), Battery Energy Storage System (BESS), Diesel Engine Generator (DEG), and Electric Vehicles (EV) using MATLAB Simulink.

2. To design a novel centralized controller for LFC of MMG i.e., Double Integral Tilt Derivative with Filter controller (DITDF) and compare its performance with Proportional–Integral–Derivative (PID), Tilt Integral Derivative with Filter (TIDF), and Integral Tilt Derivative with Filter controller (ITDF).
3. To design a novel Shrewd Sine–Cosine Algorithm (SSCA) and find optimal parameters of DITDF/ITDF/TIDF/PID, controllers.
4. To delineate the advantages of SSCA over classical SCA, recent modified SCA and some popular algorithms via varied benchmark tests.
5. To show the effectiveness SSCA for tuning of controller parameters, and contrast its outcomes with SCA, PSO and GA.
6. To examine the robustness of the suggested SSCA-DITDF control strategy via sensitivity analysis.

The remainder of the paper is divided into four sections. After the introduction, the MMG system under study is described in Section 2. The design methodology of the novel DITDF controller is elucidated in Section 3. Section 4 sets out to describe the proposed SSCA. The detailed result and analysis to vindicate the efficacy of the proposed DITDF controller and SSCA is provided in Section 5. Finally, the conclusion in Section 5 to close the manuscript.

2. System Under Study

The MMG considered for the analysis purpose in the present work is a two-area interconnected MG. The two-area MG system considered in the study consists of WTG, MT, DEG BESS, EV and UC in respectively area-1 and PV, MT, DEG, BESS, EV and UC respectively in area-2 as shown in Fig. 1. Similar, MMG transfer function structures have been considered by varied researchers [8 -9, 14, 17 – 18, 23]. In the two-area model, positive (+) symbol denotes supplying

power to the MG system, while negative (-) symbol denotes absorbing power from the MG system. Moreover, **(+ \ -)** sign in Fig. 1 indicates that these components can act as load/source of electrical energy. The components of MG as given below:

2.1 Wind Turbine Generator (WTG)

A WTG is used in an electrical generation system to transform kinetic energy from the wind into mechanical energy, subsequently utilized to generate electricity. WTG provide clean and green energy and are the primary source of power in the MG system.

The transfer function (T/F) model of WTG is expressed as:

$$G_W(\mathrm{s}) = \frac{\Delta P_{WTG}(s)}{\Delta P_W(s)} = \frac{K_{WTG}}{1+sT_{WTG}} \quad (1)$$

Where, ΔP_W = variation in WTG input power, ΔP_{WTG} = variation in WTG output power, T_{WTG} = WTG's time constant, K_{WTG}= WTG's gain.

2.2 Photo Voltaic Cell (PV)

The abundance of solar irradiance and ease of installation makes the solar PV system one of the most preferred choice among the renewable sources used in MG. A photovoltaic array is a network of solar panels that work together to convert sunshine into electricity because a single module cannot create enough power to meet all of your needs. PV Array creates electricity with no moving components, is quiet, emits no pollutants, and requires no maintenance. PV along with WTG acts as primary source of power in a MG system.

The T/F model of PV is expressed as

$$G_{PV}(\mathrm{s}) = \frac{\Delta P_{PV}(s)}{\Delta P_{\emptyset}(s)} = \frac{K_{PV}}{1+sT_{PV}} \quad (2)$$

where $\Delta P_{\emptyset}$ = variation in PV input power, ΔP_{PV} = variation in PV output power, T_{PV} = PV's time constant, K_{PV} = PV's gain.

2.3 Battery Energy Storage System (BESS)

Because of its high energy density and quick access time, BESS acts as an excellent Energy Storage System (ESS) for storing renewable energy. BESS can swiftly deliver massive amounts of electricity to the system or store a big amount of energy for a longer length of time. It comprises two main parts - a power converter and a battery bank. The role of the power converter is to provide connection between the battery bank and autonomous utility grid. The BESS receives control signals from the controller and charges/discharges energy from or to the MG, depending on whether there is an abundance or insufficient amount of energy availability.

The T/F model of BESS is expressed as

$$G_{FC}(\mathrm{s}) = \frac{\Delta P_{BESS}(s)}{\Delta P_B(s)} = \frac{K_{BESS}}{1+sT_{BESS}} \tag{3}$$

where ΔP_B = variation in BESS input power, ΔP_{BESS} = variation in BESS output power, T_{BESS} = BESS's time constant, K_{BESS} = BESS's gain.

2.4 Ultra Capacitor (UC)

Another new technology for ESS is the UC, which is also known as a supercapacitor. The charge is stored in a double layer formed on a large surface area of a microporous substance such as activated carbon. As a result, it's also known as a two-layer capacitor. UC has a variety of advantages over batteries, including a good charge/discharge efficiency, high-power density, and a longer lifecycle. Furthermore, their manufacturing costs are steadily declining. When used in conjunction with batteries, UC provides a high-power source with a longer operating duration. This is the second type of ESS used in the MMG system designed for analysis in this manuscript.

The T/F model of UC is expressed as

$$G_{UC}(\mathrm{s}) = \frac{\Delta P_{UC}(s)}{\Delta P_U(s)} = \frac{K_{UC}}{1+sT_{UC}} \tag{4}$$

Where, ΔP_U = variation in UC input power, ΔP_{UC} = variation in UC output power, T_{UC} = U C's time constant, K_{UC} = UC's gain.

2.5 Electric Vehicle (EV)

The battery of an EV has a fast response time, which provides EVs with the ability to stabilize load and frequency changes. Moreover, when connected to the grid, hundreds of EVs can operate as a big power plant. As a result, EVs can be integrated into a MG to participate in the LFC and assist power units in quickly suppressing load variations [41].

The T/F model of EV is expressed as

$$G_{EV}(\mathrm{s}) = \frac{\Delta P_{EV}(s)}{\Delta P_E(s)} = \frac{K_{EV}}{1+sT_{EV}} \tag{5}$$

Where, ΔP_E = variation in EV input power, ΔP_{EV} = variation in EV output power, T_{EV} = EV's time constant, K_{EV}= EV's gain.

2.6 Micro Turbine (MT)

Microturbines, unlike standard backup generators like DEG, are designed to run for long periods with no maintenance. They provide the base-load needs of customers, as well as be used for peak shaving, standby and cogeneration. They are used as primary back-up system in MG.

The T/F model of MT is expressed as

$$G_{MT}(\mathrm{s}) = \frac{\Delta P_{MT}(s)}{\Delta P_M(s)} = \frac{K_{MT}}{1+sT_{MT}} \tag{6}$$

where ΔP_M = variation in MT input power, ΔP_{MT} = variation in MT output power, T_{MT} = time constant of MT system, K_{MT}= MT's gain.

2.7 Diesel Engine Generator (DEG)

DEG primarily uses fossil fuels to generate electricity. In a conventional MG system, the primary source of power is WTG and PV. However, these sources are unreliable in nature. To reduce the

power discrepancy between demand and supply, the (DEG) can deliver the deficient power. DEG acts as an emergency backup system in the MG systems.

The T/F model of DEG is expressed as:

$$G_W(\mathrm{s}) = \frac{\Delta P_{DEG}(s)}{\Delta P_D(s)} = \frac{K_{DEG}}{1+sT_{DEG}} \quad (7)$$

Where, ΔP_D = incremental change in DEG input power, ΔP_{DEG} = change in DEG output power, T_{DEG} = time constant of DEG, K_{DEG} = gain of DEG.

2.8 Power and Frequency Deviation

To provide a dependable power supply, the generated power is needed to be properly controlled and must produce a stable output. However, the behavior of nonconventional power sources is unpredictable. As a result, power control scheme is anticipated to eradicate the deviation of power supply (P_s) and the required load (P_L). The power control scheme is achieved by the following condition as shown below:

$$\Delta \mathrm{P_e} = \mathrm{P_s} - \mathrm{P_L} \quad (8)$$

The total power generated by the components of the described model is denoted by P_s, while the desired demand is denoted by P_L. Frequency fluctuations are caused by the net power deviation. The model frequency deviation (Δf) is calculated in this way.

$$\Delta f = \frac{\Delta P_e}{\Delta K_{sys}+D} \quad (9)$$

The system frequency characteristics constant, ΔK_{sys}, is a constant that represents the system's frequency characteristics. As a result, the model's T/F representation is represented as

$$\mathrm{G_{SYS}(s)} = \frac{\Delta \mathrm{f}}{\Delta \mathrm{P_e}} = \frac{1}{\mathrm{Ms+D}} \quad (10)$$

In which, D = 0.12 and M = 0.2 are the suggested MG system's corresponding damping coefficient and inertia coefficient, respectively. The droop coefficient (R = R1 = R2) is set to 0.5

in this article. The frequency bias (B = B1 = B2) is taken to be 20.12. The transfer function model of two-area proposed microgrid system is illustrated in Fig. 1. All other relevant data are provided in the Appendix.

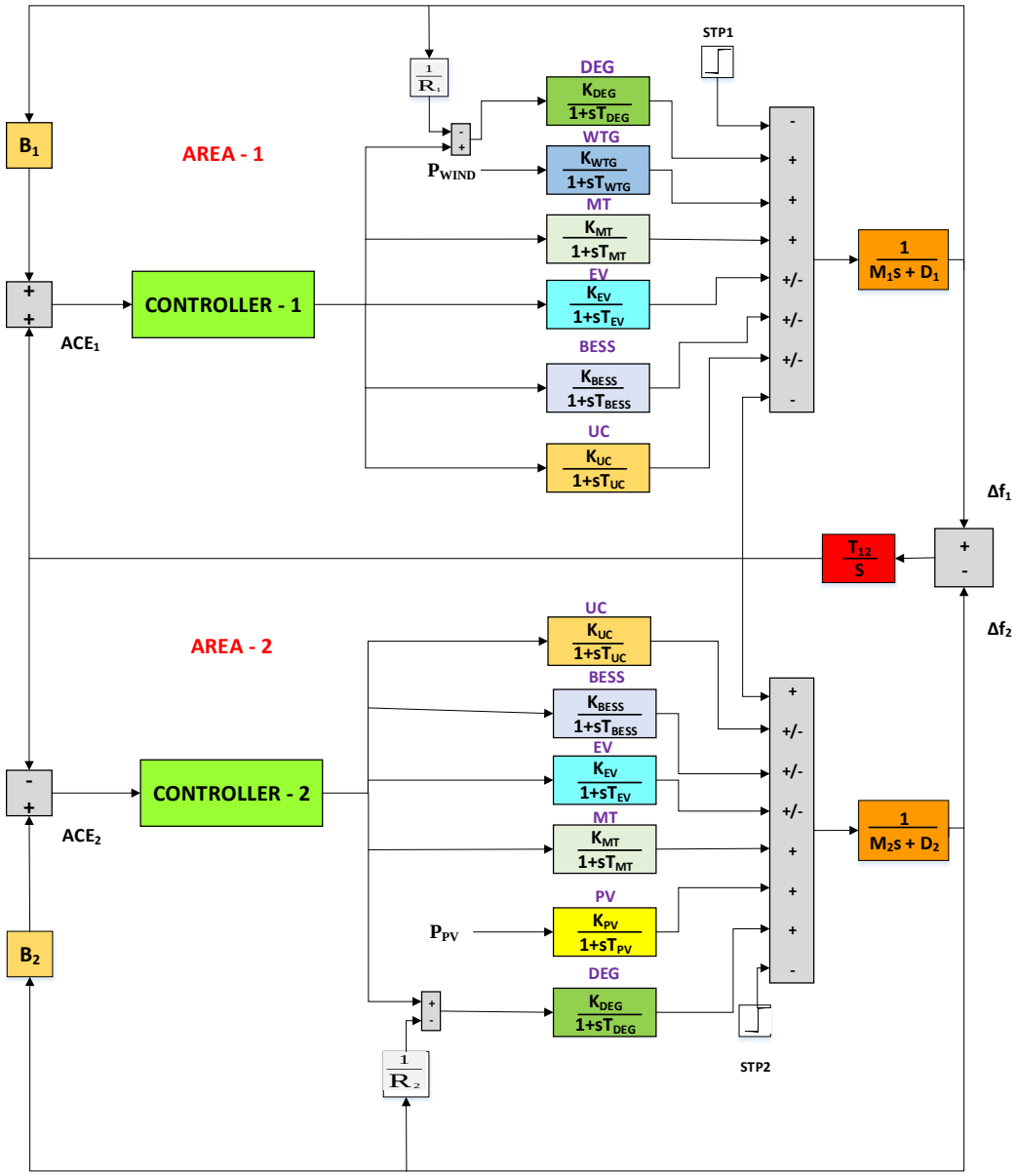

Fig. 1: Transfer Function Model of two-area MG system

3. Double Integral Tilt Derivative with Filter Controller (DITDF)

The PID controllers has been conventionally preferred for most industrial applications. However, the effects of the proportional and the derivative kicks are significant downsides of the parallel PID controllers. In [42], the researcher has suggested using an IPD controller to overcome such disadvantages and thus eliminate the immediate spiky alteration in the control signal resulting from the variation in reference input. The design language of the proposed DITDF controller has been inspired from the IPD and the TIDF controller. Hence, it possesses the benefits of the fractional order controller, tilt controller, and IPD controller. Moreover, Integral controllers, though reduces relative stability, eliminates the steady state error and improves the steady state response. Hence the presence of double integral action further improves the steady-state performance of the controller. The practicability of implementation of double integral action in controllers has already been studied by researchers [43-45]. In the DITDF controller, the integral part is directly corresponding to the ΔACE signal and the ΔF of the system is provided to the TIDF part of the control structure. The output expression of the DITDF controller is given by:

$$\Delta U = \left(\frac{K_i}{s}\right) \cdot \Delta\text{ACE} + \left(\frac{K_p}{s^{1/n}} + \frac{K_{ii}}{s} + K_d \frac{Ns}{N+s}\right) \cdot \Delta f \tag{11}$$

Where, K_p, K_d, K_i/K_{ii}, n and N are proportional, derivative, integral gain, tilt component and derivative filter coefficient, respectively.

In this manuscript, the practicability of the novel DITDF controller is examined by its implementation for the purpose of the LFC. The proposed DITDF controller has never been analyzed to the best of our knowledge, demonstrating its design novelty. The block diagram representation of the DITDF controller is illustrated in Fig. 2.

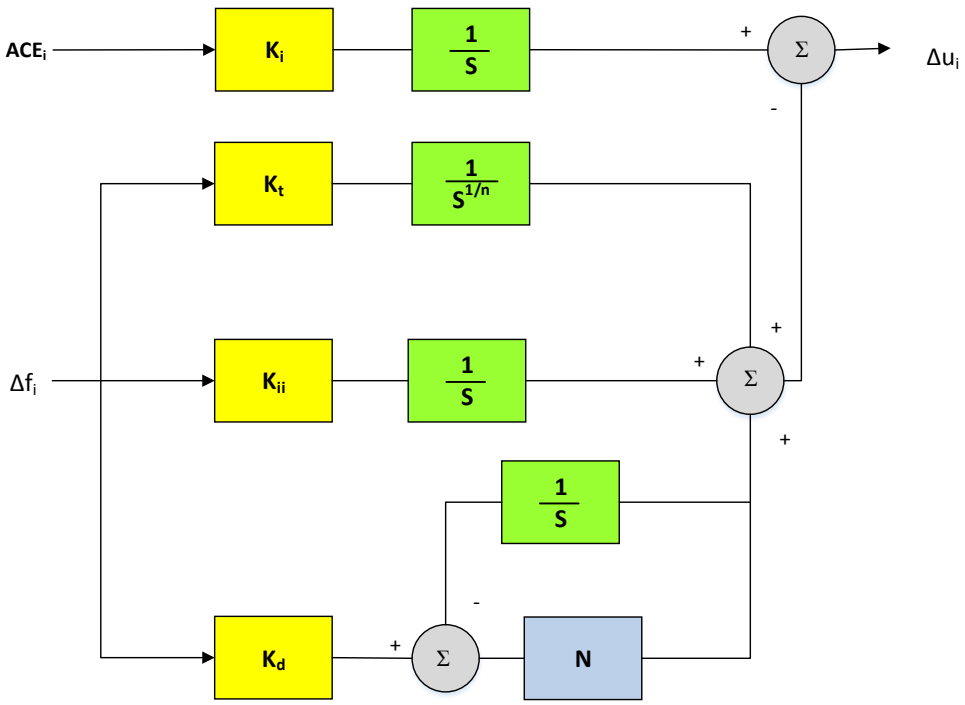

Fig. 2: Block diagram of the DITDF controller

4. Shrewd Sine–Cosine Algorithm (SSCA)

4.1 Sine–Cosine Algorithm (SCA)

In the field of stochastic optimization, SCA is a recently developed population-based meta-heuristic algorithm, which is built on the mathematical features of sine and cosine trigonometric functions. SCA, like other population-based meta-heuristic optimization methods, starts the optimization process with a set of random solutions. The objective function evaluates and updates the arbitrary set using a set of unique rules on a regular basis. As we locate the optima of optimization problems stochastically, there is no guarantee that the final result will be detected in a single run, but with several stages and random solutions, the probability of discovering the global optimum grows. During the process, the algorithm always remembers the best outcomes thus far and treats them as solution destination points. Different solutions are updated in response

to sine and cosine functions in order to find new ones. The algorithm's optimization phase is completed once the maximum iterations has been reached. The following are the search equations that are used in the SCA:

$$X_i^{t+1} = \begin{cases} X_i^t + r_1 \times \sin(r_2) \times |r_3 P_i^t - X_i^t|, & r_4 < 0.5 \\ X_i^t + r_1 \times cos(r_2) \times |r_3 P_i^t - X_{ii}^t|, & r_4 \geq 0.5 \end{cases} \quad (12)$$

where X_i^t and X_i^{t+1} represents the i^{th} solution vector at t^{th} and $(t + 1)^{th}$ iteration respectively. P_i^t is the fittest solution in the solution set.

The r1 parameter stipulates the next location regions (or movement direction), which might be within or outside of the space between the solution and the goal. The r1 can be mathematically formulated as:

$$r_1 = a - t\frac{a}{T} \quad (13)$$

In the above equation, where T denotes the maximum iterations, t denotes the current iteration, and a denotes the constant. The r_2 option specifies how far the movement should be in the direction of the goal or outwards. The r_3 option allocates random weights to the destination in order to stochastically emphasize ($r_3 > 1$) or deemphasize ($r_3<1$) the desalination effect in determining the distance. Finally, the r_4 parameter alternates between sine and cosine components equally.

The traditional SCA is effective at quickly identifying new search regions of the solution space compared to most of the other meta-heuristic algorithms. However, it is ineffective in conducting a local search around the best places gained thus far. Furthermore, in some circumstances, the SCA's candidate solutions converge to the local optimum. Thus, the classical SCA has the tendency to get stuck at the local optimum solution. As a result, to address this entrapment

problem and increase the SCA's overall performance, the original SCA needs modification. Citing the need for improvement, recently, some modified version of SCA has been published like m-SCA[35], ISCA[36], MSCA[37], OBSCA[38], HGWOSCA[39], and SCA-PSO[40]. Although the above modifications have improved the algorithm's search strategy, these updated variations are still unable to identify the optimal or near-optimal solution in some circumstances due to a lack of exploitation and exploration of the solution space. As an alternate, the current research suggests a modified version of the SCA, namely Shrewd Sine–Cosine Algorithm (SSCA), that incorporates some novel strategies to improve SSCA performance over its counterparts.

4.2 Shrewd Sine–Cosine Algorithm (SSCA)

The SSCA is an intelligent meta-heuristic algorithm designed by the modification of the classical SCA algorithm. It aims to deal with the drawbacks of the SCA and provide an improved performance, while retaining the core valuable traits of the traditional SCA. The SCA efficiently discovers the search space, however it, like other population-based algorithms, occasionally encounters an excess of the exploration. If the algorithm lacks an suitable balance between exploration and exploitation, the excess of diversity skips the genuine solutions to the problem. The solution is updated all around present state of a solution in the SCA search equations, and the area of a search space is determined by the coefficient r1, which defines transitioning from the exploration phase to the exploitation phase. The solutions are redistributed far from the current state in the prior generation of an algorithm because the coefficient r1 encourages the exploration of the search space. The greater the value of r1, the easier it is to explore the solution space, while the lower the value of r1, the easier it is to exploit the solution space locally. This value must be chosen carefully in order to achieve a balance between global exploration and

local exploitation. Moreover, our studies of the algorithm's performance revealed that this r1 parameter is altered linearly in the classical SCA, although many situations necessitate non-linear changes in an algorithm's exploratory and exploitative behaviors to avoid locally optimum solutions. Therefore, the r1 parameter needs modification.

It is also discovered that while employing the non-linear control parameter in SCA, the accuracy of solutions acquired in the last iteration could be endangered due to declining exploitation around the current elite solution space. Thus, the search equation is also modified in the SSCA. This will also facilitate to boost the exploitation of search space using personal best solution memory and supply a guidance along the population's fittest solution.

The following are the modifications that have been proposed in SSCA:

i. The search equation presented in the SCA has been modified as shown in (14):

$$X_i^{t+1} = \begin{cases} [X_i^t + r_1' \times \sin(r_2) \times |r_3 P_i^t - X_i^t|] \times F, & r_4 < 0.5 \\ [X_i^t + r_1' \times cos(r_2) \times |r_3 P_i^t - X_{ii}^t|] \times F, & r_4 \geq 0.5 \end{cases} \quad (14)$$

ii. The *F* vector introduced in the search equation is mathematically formulated as shown in (15):

$$\mathrm{F} = 1 - 0.5 \times \frac{t}{T} \quad (15)$$

iii. The r_1' is the modification of r_1 coefficient presented in the SCA, which is shown in (16):

$$r_1' = a - \sin(t\frac{a}{T}) \quad (16)$$

Where, X_i^t and X_i^{t+1} represents the i^{th} solution vector at t^{th} and $(t+1)^{th}$ iteration respectively. P_i^t is the fittest solution in the solution set. *a* is a constant and *T* is the maximum number of

iterations. The r1', r2, r3 and r4 denotes the the random numbers. The mechanism of SSCA algorithm is similar to the classical SCA but with incorporation of modifications as presented in equations (14)-(16). The Algorithm 1 provides a step-by-step description of the SSCA algorithm.

Algorithm 1: **Shrewd Sine–Cosine Algorithm (SSCA)**

1. Provide the population size P and the maximum iterations T.
2. Randomly initialize the population X_i (i= 1, 2,..., P) inside the solution space specified.
3. Determine the fitness of each unique solution.
4. Choose the best solution from the multiple candidates.
5. Set the iteration number to t=0.
6. **While** t < T **do**
7. **for** each candidate solution **do**
8. Update the r2, r3, and r4.
9. Update the value of r_1' as in (16) and F as in (15).
10. Update the position of search agents using (14).
11. Evaluate the fitness of updated solution.
12. Update the best solution.
13. **end for**
14. t = t + 1
15. **end While**
16. Return the best solution obtained so far, this is the global optimum

5. Results and Discussion

5.1 Technique Stage

This section deals with illustrating the effectiveness of the SSCA.

5.1.1 Performance Assessment of SSCA

Benchmark test functions have historically been used to evaluate the performance of metaheuristic algorithms. Benchmark functions are a collection of numerical optimization problems, and the algorithm that performs well on these functions is considered an efficacious method for solving real-world problems. This section establishes the efficacy of the proposed algorithm on a set of 20 benchmark test functions, which are available in the literature [26].

To compare the outcomes of the proposed SSCA with those of the SCA and other algorithms. The maximum number of iterations is set to 500 and the population size is chosen as 30. As a result, there are a total of 15,000 function evaluations employed in all the algorithms. The statistical results (average and standard deviation) obtained with SSCA, SCA and other popular algorithms (GA, PSO, SSA, GSA, GWO and EO referred from [29]) are reported in Tables 1. It should be emphasized that all methods are compared with the same floating-point precision, therefore any differences in results are related to the method's performance.

The first category covers unimodal functions (F_1-F_7) that have a single optimum solution and are designed to test the algorithm's exploitation ability. The SSCA completely outperforms the SCA, PSO, GA, GWO, SSA, GSA and EO in these the problems (F_1-F_5, F_7). The performance SSCA on, F_6 is better compared to the GA, PSO, and GWO. Thus, suggesting the increased exploitation ability of the purposed modification. Multi-modal functions (F_8-F_{13}), which have multiple optimal solutions, fall into the second category. Local optimal solutions in these

functions measure the algorithm's exploration performance, however to locate the global optima, an algorithm must be able to search the space worldwide and avoid getting caught in local optima. The SSCA completely outperforms the SCA in all benchmark functions in the second category (F_8-F_{13}). This suggests the superior the exploration and local optima avoidance ability of SSCA over the traditional SCA. In case of other algorithms, SSCA outperforms the likes of PSO, GA GWO, SSA, GSA and EO in the F_9-F_{11}. In F_{12} and F_{13}, the SSCA achieves a ranking of 2nd and 3rd, respectively. Fixed-dimensional multi-modal functions (F_{14}-F_{20}), which are similar to multi-modal functions but have low and fixed dimensions, fall into the third category. In this category, the SSCA again completely outperforms the SCA in all the functions (F_{14}-F_{20}). In case of the other algorithm, the SSCA ranks 1st in F_{14} - F_{17} and for the remaining (F_{18}- F_{20}), the SSCA remains fairly competitive.

Table 1: Comparison of results obtained by the SSCA, classical SCA and other popular algorithms in benchmark test.

Function		SSCA	SCA	GA [29]	PSO [29]	SSA [29]	GSA [29]	GWO [29]	EO [29]
F_1	Ave	1.51E-149	1.58E-10	0.55492	9.59E-06	1.58E-07	2.53E-16	6.59E-28	3.32E-40
	Std	2.35 E-148	2.18E-09	1.23010	3.35E-05	1.71E-07	9.67E-17	1.58E-28	6.78E-40
F_2	Ave	6.39E-82	2.67E-09	0.00566	0.02560	2.66293	0.05565	7.18E-17	7.12E-23
	Std	1.12E-80	1.19E-08	0.01443	0.04595	1.66802	0.19404	7.28E-17	6.36E-23
F_3	Ave	3.76E-124	0.01746	846.344	82.2687	1709.94	896.534	3.29E-06	8.06E-09
	Std	7.23E-123	0.13851	161.499	97.2105	11242.3	318.955	1.61E-05	1.60E-08
F_4	Ave	8.36E-69	0.00111	4.55538	4.26128	11.6741	7.35487	5.61E-07	5.39E-10
	Std	9.95E-68	0.00529	0.59153	0.67730	4.1792	1.74145	1.04E-06	1.38E-09
F_5	Ave	7.456709	7.69862	268.248	92.4310	296.125	67.5430	26.81258	25.32331
	Std	0.38376	4.81152	337.693	74.4794	508.863	62.2253	0.793246	0.169578
F_6	Ave	0.48435	0.45919	0.56250	8.89E-06	1.80E-07	2.5E-16	0.816579	8.29E-06
	Std	0.15498	0.15535	1.71977	9.91E-06	8.00E-07	1.74E-16	0.482126	5.02E-06
F_7	Ave	0.00015	0.00281	0.04293	0.02724	0.1757	0.08944	0.002213	0.001171
	Std	0.00015	0.00315	0.00594	0.00804	0.0629	0.04339	0.001996	6.54E-04
F_8	Ave	-2118.51	-2161.78	-10546.1	-6075.85	-7455.8	-2821.1	-6123.1	-9016.34

	Std	1.66E+02	1.67E+02	353.158	754.632	772.811	493.037	909.865	595.1113
F_9	Ave	0	1.35188	30.8229	52.8322	58.3708	25.9684	0.31052	0
	Std	0	5.24438	7.57295	16.7068	20.016	7.47006	0.35214	0
F_{10}	Ave	8.88E-16	0.04251	1.63551	0.00501	2.6796	0.06208	1.06E-13	8.34E-14
	Std	0	0.71859	0.46224	0.01257	0.8275	0.23628	2.24E-13	2.53E-14
F_{11}	Ave	0	0.08819	0.56112	0.02381	0.0160	27.7015	0.00448	0
	Std	0	0.16103	0.26942	0.02870	0.0112	5.04034	0.00665	0
F_{12}	Ave	0.02130	0.09768	0.03088	0.02764	6.9915	1.79961	0.05343	7.97E-07
	Std	0.02003	0.06230	0.04092	0.05399	4.4175	0.95114	0.02073	7.69E-07
F_{13}	Ave	0.22678	0.33895	0.36222	0.00732	15.8757	8.89908	0.65446	0.029295
	Std	0.08284	0.09750	0.30975	0.01050	16.1462	7.12624	0.00447	0.035271
F_{14}	Ave	0.99800	1.84986	0.998004	3.84902	1.1965	5.859838	4.042493	0.998004
	Std	0.92043	1.50009	4.23E-12	3.24864	0.5467	3.831299	4.252799	1.54E-16
F_{15}	Ave	0.00076	0.00110	0.005206	0.002434	0.000886	0.003673	0.00337	0.002398
	Std	0.00030	0.00036	0.007028	0.006081	0.000257	0.001647	0.00625	0.035271
F_{16}	Ave	-1.03164	-1.03158	-1.03162	-1.03162	-1.03163	-1.03163	-1.03163	-1.03162
	Std	8.89E-05	5.75E-05	1.34E-06	6.51E-16	6.13E-14	4.88E-16	2.13E-08	6.04E-16
F_{17}	Ave	0.39719	0.40077	0.397890	0.397887	0.397887	0.397887	0.397889	0.397887
	Std	0.00027	0.00394	1.08E-05	0	3.41E-14	0	2.13E-04	0
F_{18}	Ave	3.00004	3.00008	3.000002	3	3	3	3.000028	3
	Std	5.24E-05	0.00015	4.06E-06	1.97E-15	2.20E-13	4.17E-15	4.24E-04	1.56E-15
F_{19}	Ave	-3.861702	-3.85435	-3.86278	-3.86278	-3.86278	-3.86278	-3.86263	-3.86278
	Std	0.003769	0.00335	1.63E-07	2.65E-15	1.47E-10	2.29E-15	0.00273	2.59E-15
F_{20}	Ave	-3.205243	-2.89481	-3.27443	-3.26651	-3.2304	-3.31778	-3.28654	-3.2687
	Std	0.345198	0.35009	0.05924	0.06032	0.0616	0.023081	0.10556	0.05701

In the next step, the SSCA is compared with the various modified SCA (discussed in section 4.1), using the same benchmark test. The statistical results (average and standard deviation) obtained with SSCA and its other modifications are presented in Table 2. The Table 2 show that the solutions obtained with SSCA are either substantially superior or extremely competitive with those of the m-SCA [35], ISCA [36], MSCA [37], OBSCA [38], HGWOSCA [39], and SCA-PSO [40]. The SSCA completely outperforms all the modifications in 13 (F_1-F_5 F_7, F_9-F_{11}, F_{13}-$F_{15,}$ $F_{17)}$ out of the total 20 benchmark functions. In the functions F_6, $F_{12,}$ and $F_{18,}$ SSCA is ranked

2^{nd}, 3^{rd} and 3^{rd}, respectively, compared to other modifications. In remaining functions, the SSCA performs competitive, providing results closer to global optimum.

Thus, the following analysis lucidly indicates the improved solution attained by the SSCA as compared to the classical SCA and the other variations of SCA. After comparing with different algorithms for unimodal, multimodal and fixed benchmark functions the SSCA algorithm is employed to a real engineering problem of LFC in MMG in the next section.

Table 2: Comparison of the performance SSCA with modified variants of SCA in benchmark test

Function		m-SCA	ISCA	MSCA	OBSCA	HGWOSCA	SCA-PSO	SSCA
F_1	Ave	3.18E-03	1.24E-29	5.87E+01	8.43E-21	5.06E-47	6.04E-11	1.51E-149
	Std	2.13E-03	1.76E-29	6.98E+01	2.76E-20	1.77E-46	1.98E-10	2.35 E-148
F_2	Ave	6.41E-05	1.76E-18	8.67E-03	7.30E-16	2.27E-28	8.85E-08	6.39E-82
	Std	3.12E-03	2.94E-18	9.76E-03	3.09E-15	2.61E-28	4.87E-08	1.12E-80
F_3	Ave	8.51E+02	7.96E-02	4.56E+02	1.98E+00	2.89E-21	9.01E+01	3.76E-124
	Std	8.76E+02	2.71E-01	5.49E+02	5.73E+00	9.66E-21	4.97E+01	7.23E-123
F_4	Ave	2.63E-02	3.81E-07	4.72E+01	5.72E-01	2.38E-14	1.87E+00	8.36E-69
	Std	3.16E-02	7.92E-07	8.48E+00	2.75E+00	4.57E-14	5.60E-01	9.95E-68
F_5	Ave	2.65E+01	1.65E+01	2.71E+05	2.57E+01	2.53E+01	4.71E+01	7.46E+00
	Std	6.87E-01	4.79E-01	5.87E+05	4.91E-01	9.64E-01	2.36E+01	3.84E-01
F_6	Ave	1.02E+00	2.71E-01	5.08E+01	3.35E+00	8.31E-01	9.78E-04	4.84E-01
	Std	3.32E-01	3.21E-01	3.92E+01	2.72E-01	2.32E-01	1.78E-04	1.55E-01
F_7	Ave	1.40E-02	1.55E-03	1.84E-01	2.81E-03	8.52E-03	3.78E-03	1.50E-04
	Std	5.76E-03	7.63E-04	1.58E-01	2.86E-03	5.62E-03	8.64E-03	1.50E-04
F_8	Ave	-2.21E+03	-1.28E+03	-3.87E+03	-3.27E+03	-2.56E+03	-7.12E+03	-2.12E+03
	Std	2.20E+03	4.16E+02	3.72E+02	7.64E+02	3.67E+02	5.83E+02	1.66E+02
F_9	Ave	3.78E+01	1.82E-01	5.18E+01	1.23E-05	4.51E+00	9.67E+00	0
	Std	3.73E+01	8.19E-01	5.90E+01	5.17E-05	4.50E+00	8.06E+00	0
F_{10}	Ave	1.71E-04	2.23E-14	2.12E+01	1.42E+01	1.23E-14	1.89E+00	8.88E-16
	Std	3.29E-03	8.47E-15	7.92E+00	9.12E+00	3.42E-15	6.14E+00	0
F_{11}	Ave	3.64E-02	1.97E-13	8.48E-01	9.26E-11	3.26E-02	1.82E-02	0
	Std	5.06E-02	8.65E-13	4.73E-01	3.48E-10	3.98E-02	1.68E-02	0
F_{12}	Ave	3.95E-01	1.75E-02	9.88E+04	4.10E-01	1.09E-02	3.01E-02	2.13E-02
	Std	7.32E-01	9.13E-03	1.41E+05	1.89E-01	1.50E-02	4.76E-02	2.00E-02

F_{13}	Ave	3.67E+00	3.03E-01	6.78E+05	4.13E+00	5.02E-01	8.93E-01	2.27E-01
	Std	2.53E+00	1.55E-01	4.62E+05	1.90E-01	2.53E-01	8.97E-02	8.28E-02
F_{14}	Ave	1.27E+00	1.02E+00	1.90E+00	2.90E+00	6.67E+00	1.52E+00	9.98E-01
	Std	1.25E-01	1.15E+00	1.01E+00	3.16E+00	4.23E+00	1.11E+00	9.20E-01
F_{15}	Ave	7.91E-03	8.10E-04	9.07E-04	9.21E-04	6.35E-03	1.62E-03	7.59E-04
	Std	7.17E-05	1.45E-04	3.10E-04	3.05E-04	9.32E-03	3.42E-03	2.99E-04
F_{16}	Ave	-1.03E+00	-1.03E+00	-1.03E+00	-1.03E+00	-1.03E+00	-1.03E+00	-1.03E+00
	Std	8.75E-07	1.94E-08	5.92E-05	8.08E-04	1.69E-09	9.75E-16	8.89E-05
F_{17}	Ave	3.98E-01	3.98E-01	3.99E-01	4.00E-01	3.98E-01	3.98E-01	3.97E-01
	Std	2.97E-05	8.12E-05	1.03E-03	3.15E-03	1.77E-07	4.86E-16	2.71E-04
F_{18}	Ave	3.00E+00	3.00E+00	3.00E+00	3.00E+00	3.00E+00	3.00E+00	3.00E+00
	Std	9.78E-05	5.46E-08	2.60E-04	2.76E-02	9.78E-05	9.94E-14	5.24E-05
F_{19}	Ave	-3.86E+00	-3.86E+00	-3.86E+00	-3.86E+00	-3.86E+00	-3.86E+00	-3.86E+00
	Std	6.74E-04	8.02E-05	4.74E-03	7.78E-03	1.44E-03	2.97E-13	3.77E-03
F_{20}	Ave	-3.32E+00	-3.28E+00	-3.06E+00	-3.07E+00	-3.27E+00	-3.27E+00	-3.21E+00
	Std	2.86E-03	4.12E-02	9.72E-02	9.78E-01	6.35E-02	8.87E-02	3.45E-01

5.1.2 Performance of SSCA in MMG system

This section focuses on establishing the superiority of the SSCA over three other intelligent algorithms (GA/PSO/SCA), irrespective of the type of controller used for LFC in the MMG. For the study, the transfer function model (Fig. 1) of the two-area MG model discussed in section 1 is considered throughout this and the future sections. For investigation of the system dynamics in this section, a step load perturbation (SLP) of 5% at t=0 sec in area1 is considered. The MMG is also provided with an incremental change in solar irradiation power (P_{PV}) = 0.3 p.u and wind power fluctuation P_{WTG} = 0.2 p.u to study frequency regulation. The optimal values of the controller parameter obtained by different algorithms is presented in Table 3.

Table 3: Optimized Parameters of Controllers using different techniques

ALGORITHM	CONTROLLER	OPTIMIZED PARAMETERS OF CONTROLLER											
		AREA1						AREA2					
		KP_1	KI_1	KI_{11}	KD_1	N_1	n_1	KP_2	KI_2	KI_{22}	KD_2	N_2	n_2

GA	PID	0.2149	1.9100	-	0.1700	-	-	1.7900	1.8400	-	0.0265	-	-
	TIDF	1.6251	1.9160	-	0.0844	550.2699	20.2	1.2934	1.9638	-	0.1428	1311.4394	17.3785
	ITDF	0.4936	-1.2505	-	0.0616	1988.1444	11.7835	0.7342	-1.9998	-	0.3297	970.7973	11.1453
	DITDF	0.3216	-0.8276	0.2182	0.1965	1279.5765	109.601	1.2689	-1.9986	0.1125	0.4587	109.6019	12.3424
PSO	PID	0.4519	1.9800	-	0.1800	-	-	1.9900	1.9600	-	0.0200	-	-
	TIDF	1.9598	1.9160	-	0.1262	2000.2	11.9527	1.5527	1.9638	-	0.2013	2000.4	13.3649
	ITDF	0.5393	-1.2302	-	0.2288	354.2156	7.0911	0.8369	-1.9981	-	0.5055	1132.8373	9.6412
	DITDF	0.6266	-0.9286	0.2382	0.1665	1229.5765	8.4401	1.3799	-1.9998	0.1125	0.5587	104.5969	12.4424
SCA	PID	0.6519	1.9800	-	0.1701	-	-	2.1000	1.9600	-	0.0200	-	-
	TIDF	1.1403	1.8050	-	0.9315	21.4523	1.5217	1.0328	1.8678	-	0.1604	2000.4	12.4102
	ITDF	0.5955	-1.4348	-	0.2771	473.5880	19.9292	0.2358	-2.0000	-	0.0621	2000.4	11.3370
	DITDF	1.9598	-1.8986	0.5234	0.4390	2000.2	20.2	1.9380	-2.0000	1.9638	0.1271	1360.7382	20.4
SSCA	PID	0.7804	1.9800	-	0.1786	-	-	1.9900	1.9600	-	0.0630	-	-
	TIDF	1.9598	1.9160	-	0.9615	23.4343	1.6357	1.9378	1.9638	-	0.1804	2000.4	12.5306
	ITDF	1.9598	-1.8990	-	1.0709	26.5579	1.7796	0.6867	-2.0000	-	0.3169	1176.7569	20.1288
	DITDF	1.9598	-1.8990	1.9160	0.9272	1985.9245	11.9688	0.4862	-2.0000	-0.1337	0.3831	8.1784	20.4

To achieve the aim of this section, First the PID controller is incorporated in the MMG model (Fig .1). It is known that controller parameters influence the performance of the controllers. Thus, to compare the effectiveness of various techniques, the parameters of the PID controller is altered as per the optimum values suggested by each technique (Table 3). In subsequent steps the TIDF, ITDF and the DITDF controller is incorporated in the same MMG, to suggest that the trend in performance of algorithms remain intact irrespective of the controller used. The dynamic responses obtained under different cases considered in this section are illustrated in Fig.3 and their respective transient response and performance index *J* (ITAE) is presented in Table 4.

The response as shown Fig. 3 clearly states that the most optimum performance was obtained when EO algorithm was used with display of better undershoot, overshoot and settling time. Firstly, when the PID controller was incorporated in the MMG, it is observed that the

performance of the SSCA exceed its counterparts SCA by 10.97%, PSO by 20.17% and GA by 27.04. Secondly, with the use of TIDF, the performance of SSCA exceeds the SCA, the PSO and the GA by 5.04%, 17.51% and 27.08%. Thirdly, with replacement of TIDF with ITDF, the SSCA performance surpasses the SCA, PSO and the GA by 29.37%, 40.97% and 49.37%. Finally, with the introduction of the DITDF controller, it is noticed the SSCA again exceeds its counterparts SCA, PSO, and GA by a margin of 24.03%, 59.48% and 68.14 %, respectively.

With all the detailed analysis and simulation results, it is safe to assert the supremacy of the SSCA over its three other counterparts. Table 4 also supports the assertions by demonstrating that the least value of transient parameters and ITAE is obtained when SSCA is used. Thus, it can be concluded that the SSCA technique is providing better system performance in stabilizing the frequency and tie-line power in the MMG system. Hence, for further analysis only the SSCA algorithm will be considered.

Table 4: Transient Response Parameters and Performance Index *J* (ITAE)

CONTROLLER	ALGORITHM	TRANSIENT RESPONSE PARAMETERS						PERFORMANCE INDEX *J* (ITAE) ($\times 10^{-2}$)
		OVERSHOOT, (pu)			UNDERSHOOT ($\times 10^{-3}$), (pu)			
		$\Delta f_1(\times 10^{-3})$	$\Delta f_2(\times 10^{-3})$	$\Delta P_{tie}(\times 10^{-3})$	$\Delta f_1(\times 10^{-3})$	$\Delta f_2(\times 10^{-5})$	$\Delta P(\times 10^{-3})_{tie}$	
PID	GA	4.324	3.421	1.169	-5.300	-6.270	-4.948	8.68
	PSO	3.454	2.541	0.2317	-5.157	-4.748	-4.292	7.92
	SCA	3.206	2.223	0.0008	-4.965	-5.369	-4.060	7.11
	SSCA	2.759	1.813	0.0002	-4.813	-3.110	-3.771	6.33
TIDF	GA	4.881	2.848	0	-7.302	-7.807	-3.893	6.46
	PSO	3.245	2.669	0.0005	-5.984	-2.716	-3.473	5.71
	SCA	1.861	2.245	0	-4.205	-1.953	-3.265	4.96
	SSCA	1.542	1.628	0	-3.986	-2.314	-3.138	4.71
ITDF	GA	8.618	3.168	0.2569	-9.827	-1.872	-4.975	4.32
	PSO	3.505	2.536	0.2552	-4.716	-0.2509	-4.348	3.71

	SCA	3.056	3.168	0.717	-3.998	-1.872	-4.470	3.10
	SSCA	1.463	1.336	0.1686	-3.574	-2.211	-3.112	2.19
DITDF	GA	4.225	2.941	0.002	-5.216	-5.952	-8.137	2.48
	PSO	3.685	1.938	2.256	-5.745	-1.752	-5.077	1.95
	SCA	1.341	1.866	0.1668	-2.612	-1.649	-4.366.	1.04
	SSCA	1.163	0.7663	0.0008	-1.378	-1.638	-2.174	0.79

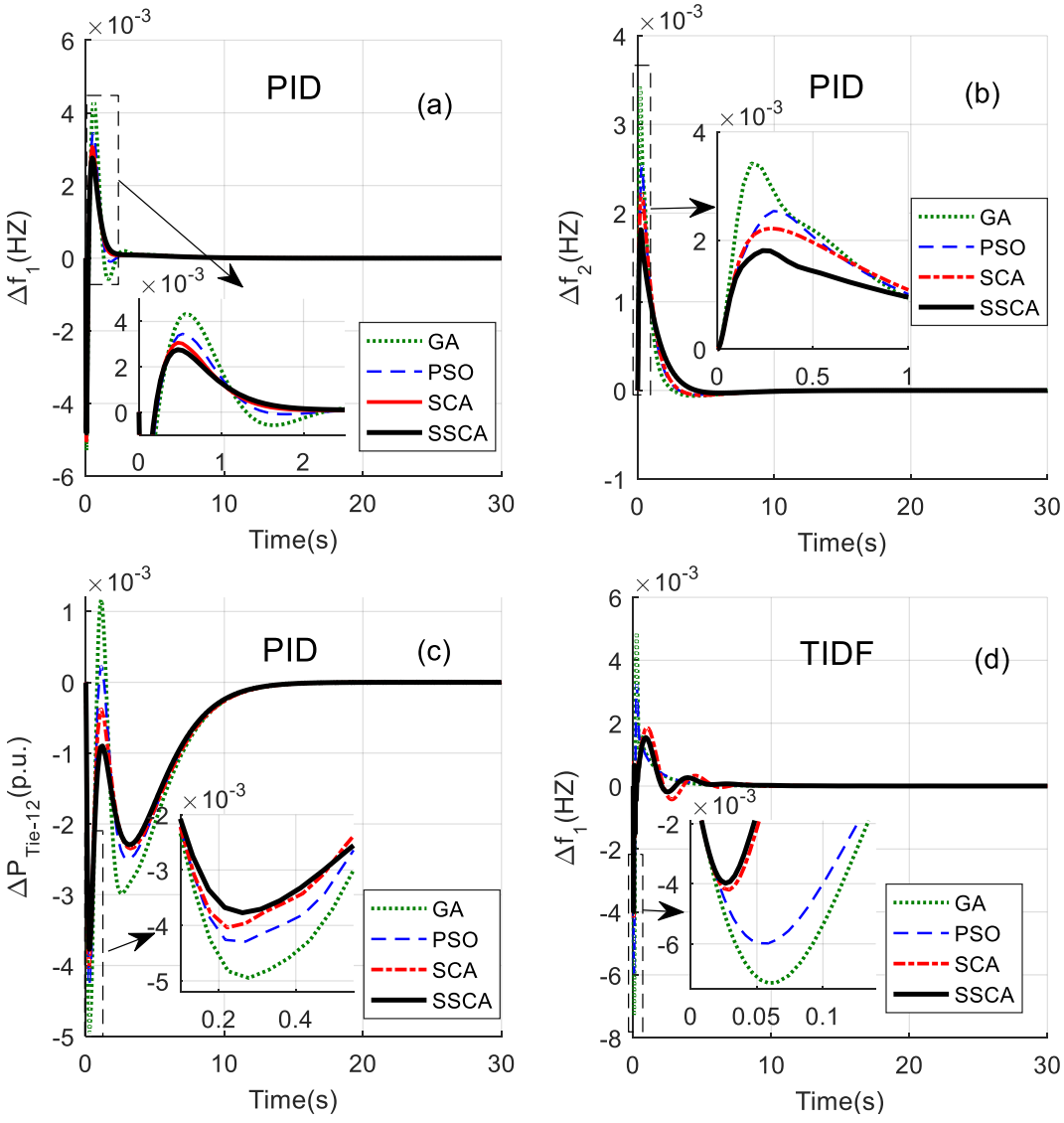

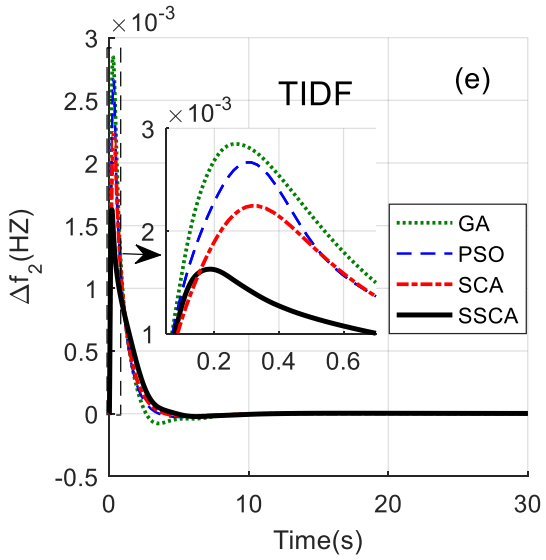
TIDF
(e)
Δf_2(HZ)
Time(s)
GA
PSO
SCA
SSCA

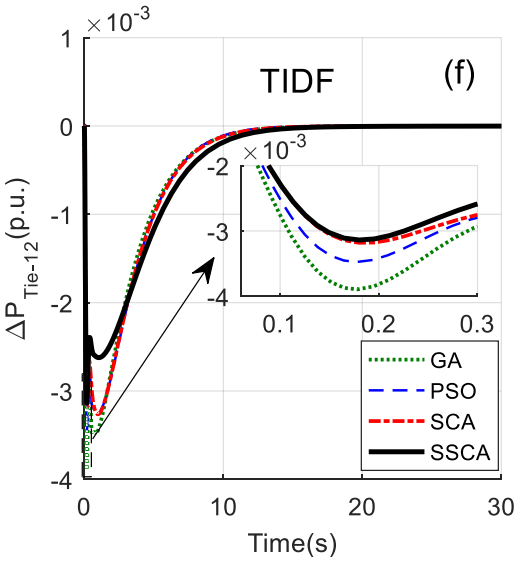
TIDF
(f)
ΔP_{Tie-12}(p.u.)
Time(s)
GA
PSO
SCA
SSCA

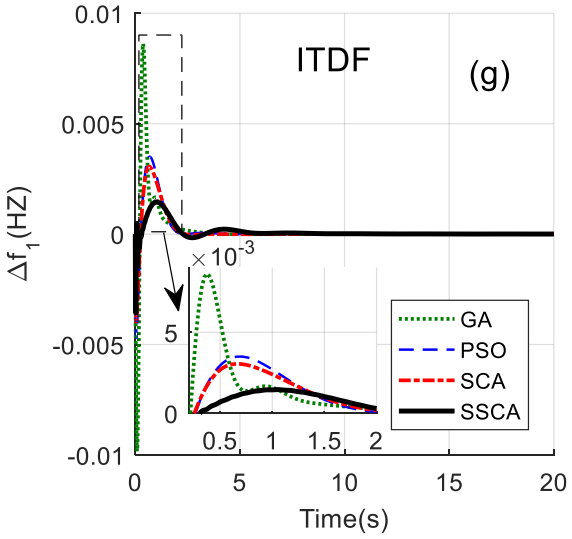
ITDF
(g)
Δf_1(HZ)
Time(s)
GA
PSO
SCA
SSCA

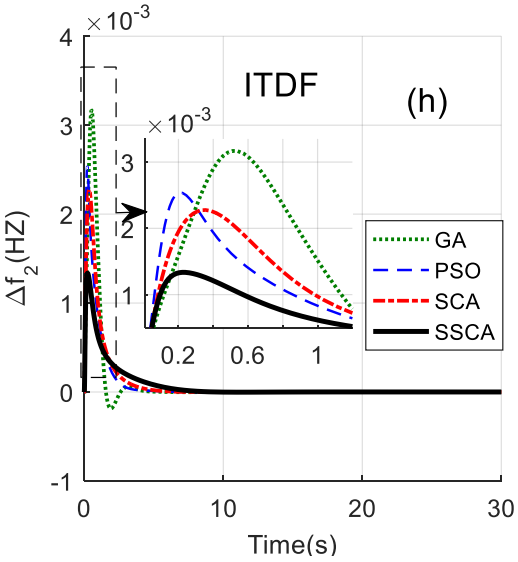
ITDF
(h)
Δf_2(HZ)
Time(s)
GA
PSO
SCA
SSCA

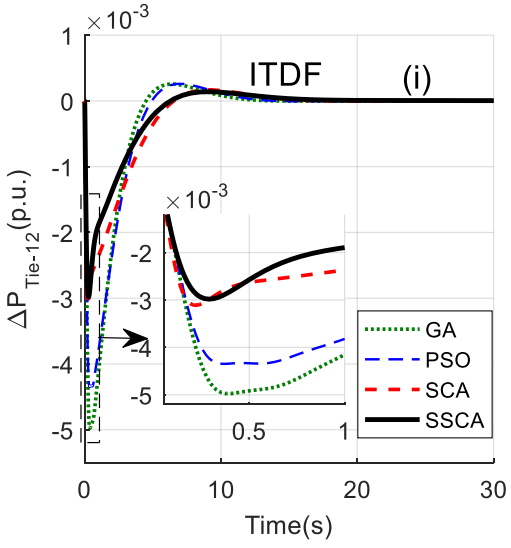
ITDF
(i)
ΔP_{Tie-12}(p.u.)
Time(s)
GA
PSO
SCA
SSCA

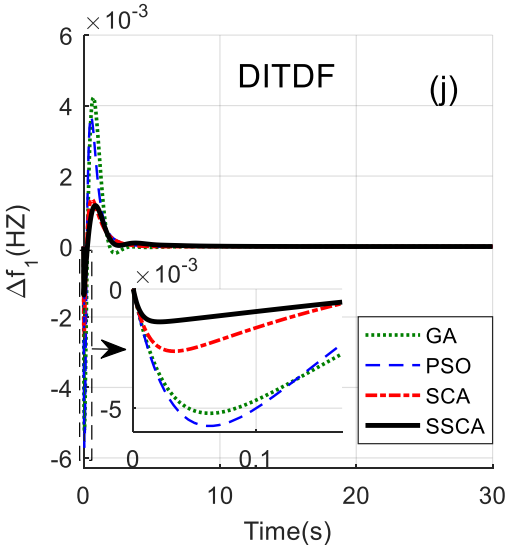
DITDF
(j)
Δf_1(HZ)
Time(s)
GA
PSO
SCA
SSCA

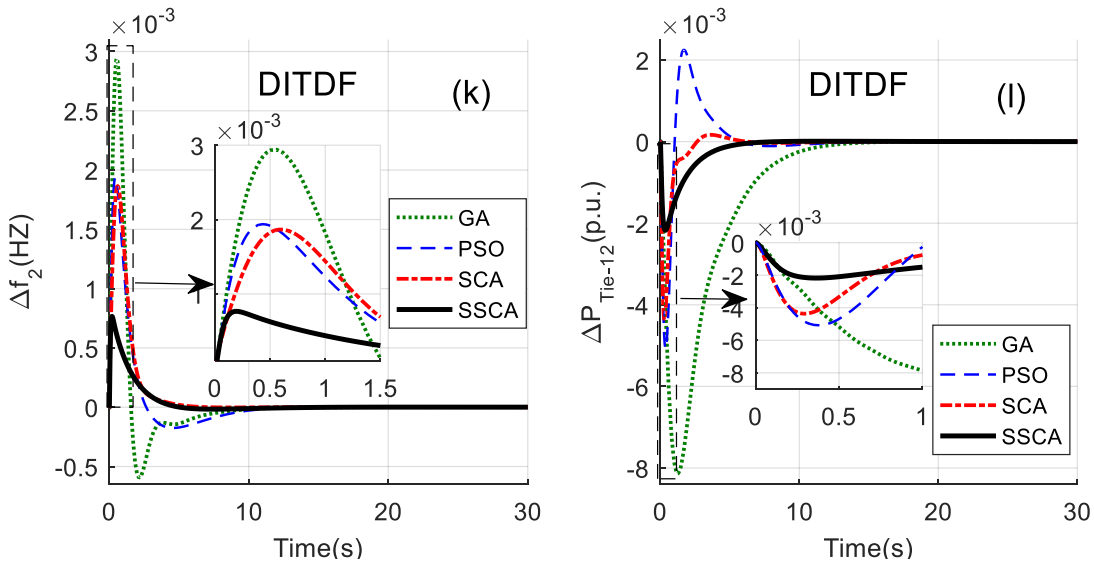

Fig. 3: Dynamic responses of MMG with **(a)-(c)** PID, **(d)-(f)** TIDF, **(g)-(i)** ITDF, **(j)-(l)** DITDF for a load variation of 5% in area1 using GA, PSO, SCA and SSCA Algorithms.

5.2 Controller Stage

This section deals with justifying the potency of the proposed DITDF controller over the PID / TIDF / ITDF controller for the purpose of LFC of the MMG system. In practice, the MMG is subject to a variety of uncertainties. Three different case studies have been conducted in this regard to assess the reliability of system performance and the feasibility of suggested approaches. These cases are formed by a different pattern of demand, solar irradiation power and wind power fluctuation. Similar cases have been considered by many researchers [15, 24, 30, 32, 38, 41]. In all the circumstances, Initially, the two-area MG is incorporated with the PID controller, and the system's dynamic response is recorded. In the succeeding stages, the PID controller is replaced with the TIDF, ITDF and DITDF controller and their performance in the MMG is registered. Following this, the performance is compared, and the best controller strategy is acknowledged. For the optimal gains of the parameter refer to Table 3.

5.2.1 Case – I: Fixed demand, variable solar and wind power

In this case, the demand is kept, but the solar and wind power are made variable. The change in P_{WTG} and P_{PV} is illustrated in Fig. 4 and Fig.5, respectively. Fig.6 (a)-(c) shows the dynamic responses obtained in case – II, and their transient response parameter with ITAE values is shown in Table 5.

Similar to Case-I, the suggested SSCA optimized DITDF controller enhances system dynamic responses significantly under the presented uncertainties, as illustrated in Fig.6. Additionally, ITAE values representing the improved performance of the MMG also suggest the same supremacy of the DITDF controller. The objective function value is decreased by 13.58%, 9.56% and 6.16% with DITDF compared to PID, TIDF and ITDF respectively.

Table 5 : Transient Response Parameters and Performance Index *J* (ITAE) for Case II.

CONTROLLER	TRANSIENT RESPONSE PARAMETERS				PERFORMANCE INDEX *J* (ITAE)
	OVERSHOOT, (pu)		UNDERSHOOT, (pu)		
	Δf_1 ($\times 10^{-4}$)	Δf_2($\times 10^{-5}$)	Δf_1($\times 10^{-3}$),	Δf_2($\times 10^{-4}$)	
PID	8.290	6.680	-5.374	-3.459	0.4312
TIDF	6.997	5.839	-4.169	-1.5489	0.4120
ITDF	5.108	5.275	-3.727	-1.847	0.3971
DITDF	3.535	2.605	-1.446	-0.2718	0.3726

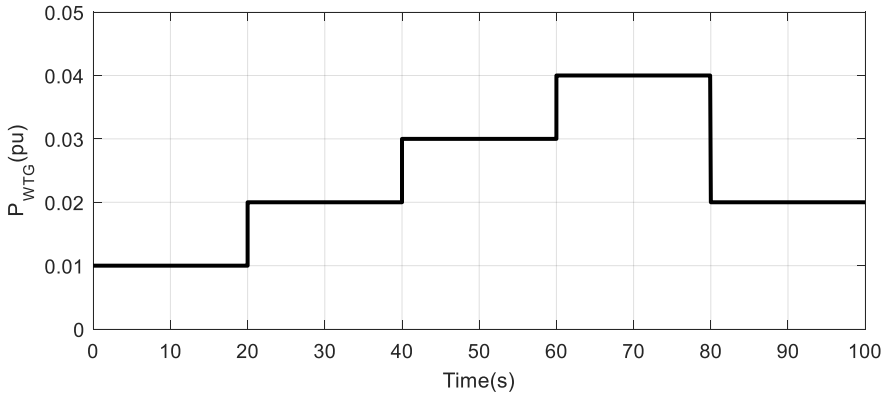

Fig 4: Wind Power Fluctuation

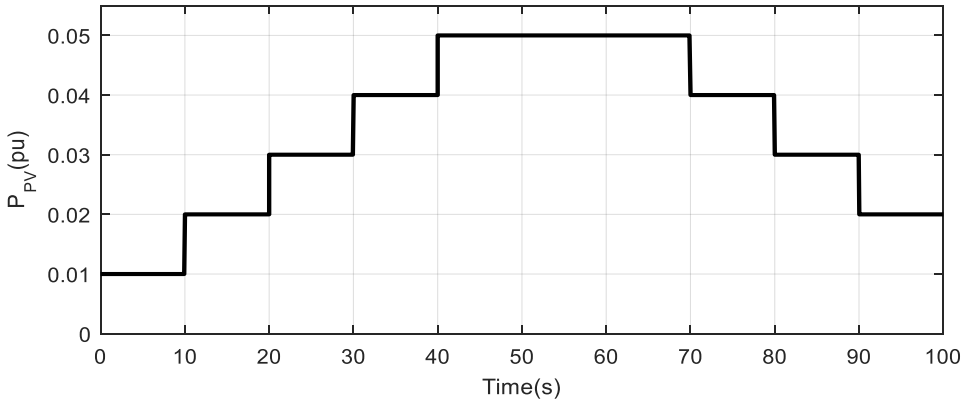

Fig. 5: Variation in solar power irradiation

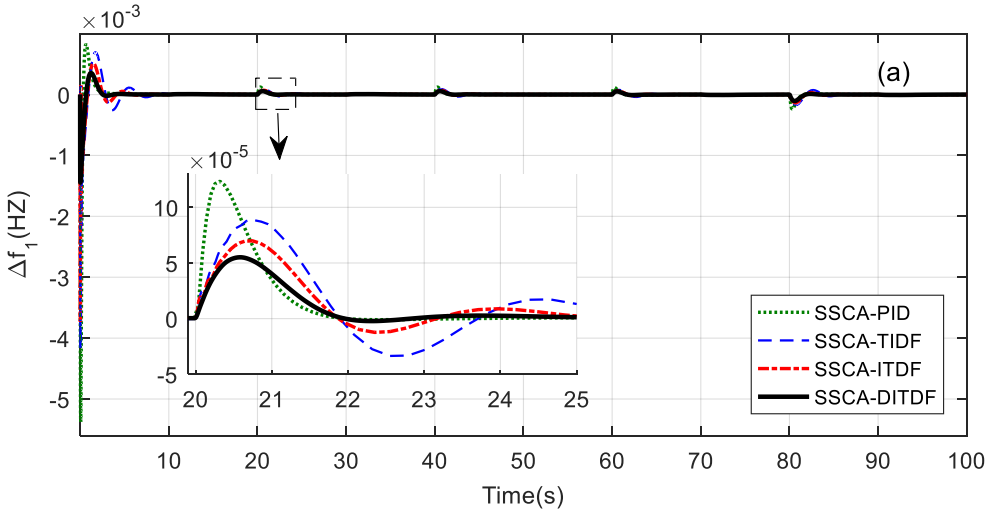

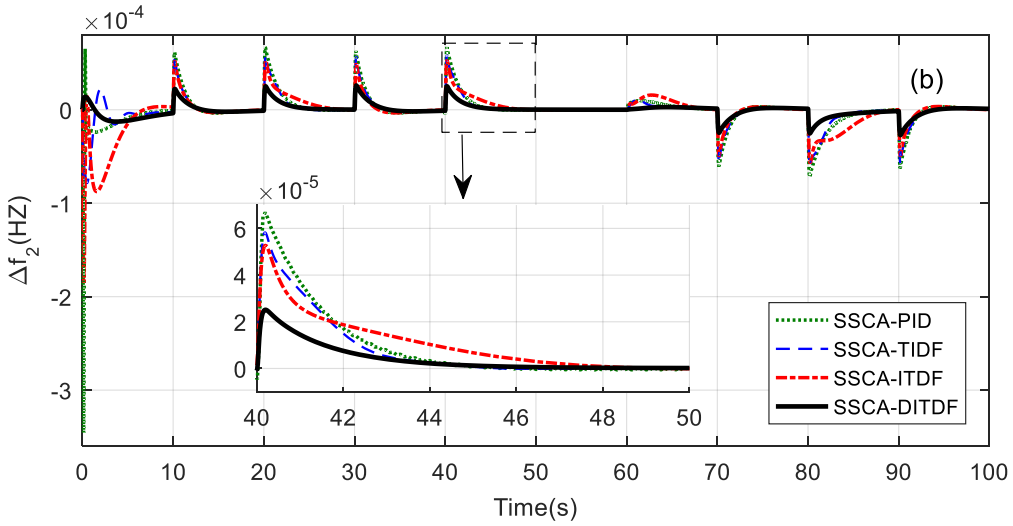

Fig. 6: Dynamic response of the MMG in **(a)** Area-1, and **(b)** Area-2 for case II.

5.2.2 Case – II: Variable demand, solar and wind power

In this case, the load demand (P_L), solar power and wind power each of these are made variable. The change in P_{PV} and P_{WTG} is similar to the previous case. The variation of P_D is shown in Fig.7. Fig.8 (a)-(c) shows the dynamic responses obtained in case – II, and their transient response parameter with ITAE values is shown in Table 6.

Similar to the previous cases, the suggested SSCA optimized DITDF provides the best response, as illustrated in Fig. 8. Furthermore, like the previous cases the SSCA based DITDF provides the least value of both the ITAE and the transient parameters. With the introduction of DITDF, the objective function value is reduced by 36.8%, 29.5% and 18.85% compared to PID, TIDF and ITDF respectively.

Table 6: Transient Response Parameters and Performance Index *J* (ITAE) for Case III.

CONTROLLER	TRANSIENT RESPONSE PARAMETERS		PERFORMANCE INDEX *J* (ITAE)
	OVERSHOOT, (pu)	UNDERSHOOT,(pu)	

	Δf_1 ($\times 10^{-3}$)	Δf_2($\times 10^{-4}$)	Δf_1($\times 10^{-3}$),	Δf_2($\times 10^{-4}$)	
PID	3.293	3.522	-6.454	-4.537	1.1721
TIDF	2.520	1.547	-5.002	-1.371	1.0502
ITDF	2.251	1.669	-4.476	-1.058	0.9123
DITDF	0.8749	0.6446	-1.736	-0.4825	0.7403

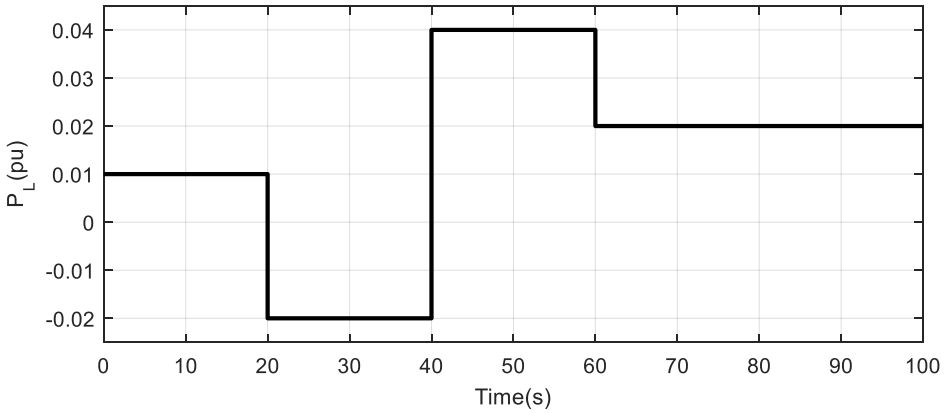

Fig. 7: Change in Load Demand

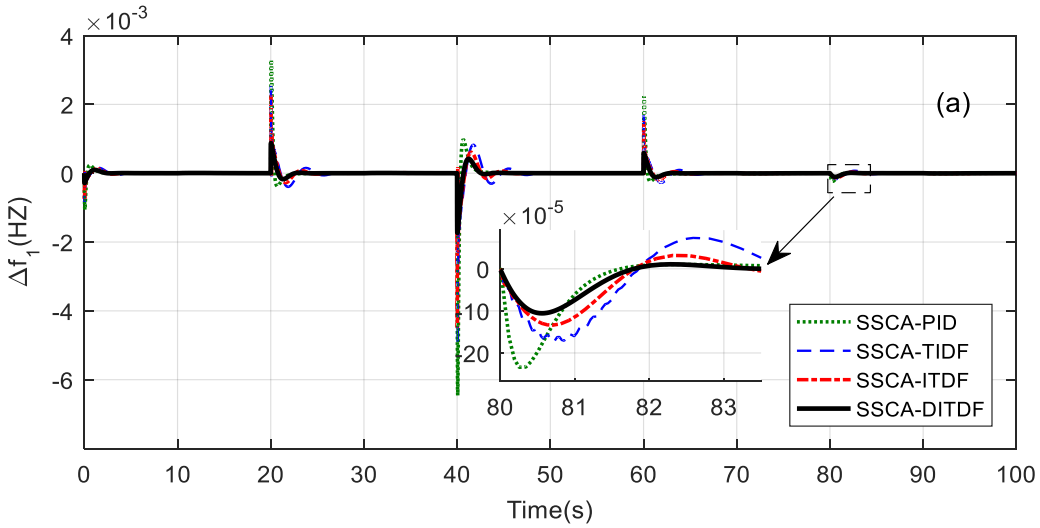

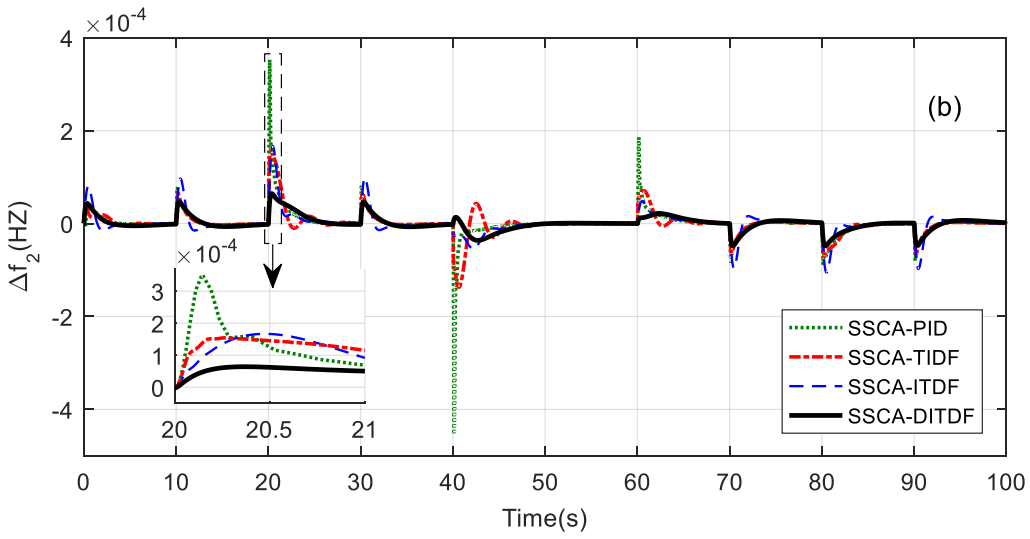

Fig. 8: Dynamic response of the MMG in **(a)** Area-1 and **(b)** Area-2 for case III.

5.2.3 Case – III: Variable demand, solar and wind power with noise

Like the previous case, the load demand (P_L), solar power and wind power variable. However, the patter of variation has included noise components, to simulate a more realistic scenario. The variation of $P_{L,}$ P_{WTG} and P_{PV} are shown in Fig.9(a)-(c). Fig.10(a)-(c) shows the dynamic responses obtained in case – III, and the numerical values of transient parameters for the aforementioned perturbations with ITAE values is shown in Table 7.

Similar to the previous cases, the suggested SSCA-DITDF surpasses its competitors and provides the best response, as illustrated in Fig. 10. Additionally, like the earlier cases, the SSCA based DITDF offers the least value of both the ITAE and the transient parameters. The performance index value is decreased by 38.78%, 32.12% and 18.99% with DITDF compared to PID, TIDF and ITDF respectively.

Table 7: Transient Response Parameters and Performance Index *J* (ITAE) for Case IV.

CONTROLLER	TRANSIENT RESPONSE PARAMETERS				PERFORMANCE INDEX *J* (ITAE)
	OVERSHOOT (pu)		UNDERSHOOT (pu)		
	Δf_1 ($\times 10^{-3}$)	Δf_2($\times 10^{-4}$)	Δf_1($\times 10^{-3}$),	Δf_2($\times 10^{-4}$)	
PID	3.274	3.397	-6.427	-4.579	1.2613
TIDF	2.554	1.517	-4.981	-1.447	1.1376
ITDF	1.437	0.6449	-4.460	-0.6771	0.9532
DITDF	0.5771	0.2597	-0.167	-0.4999	0.7721

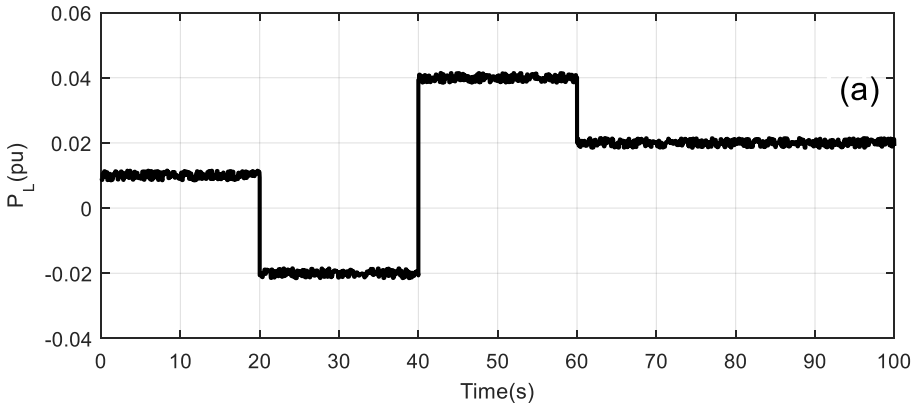

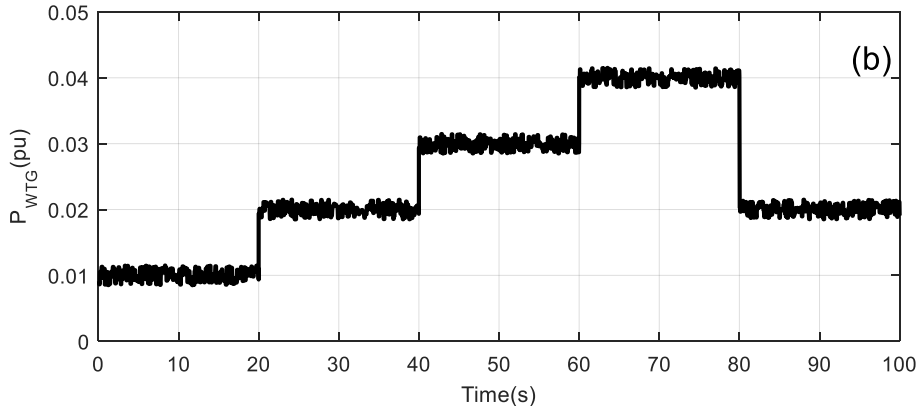

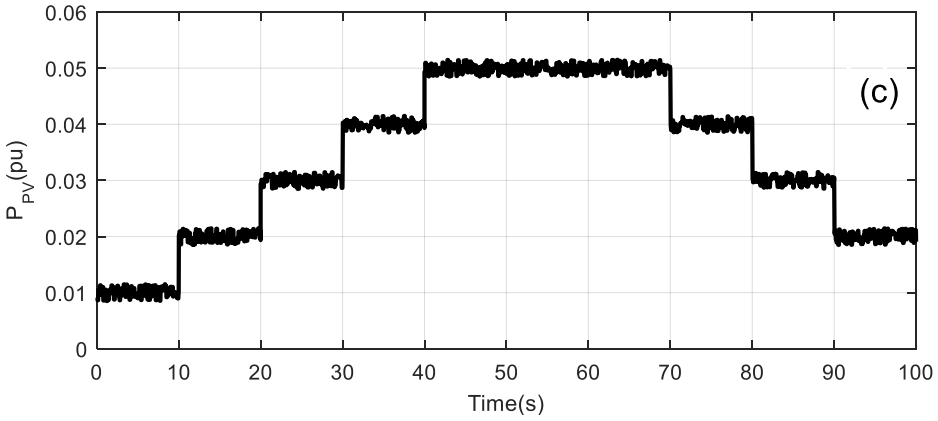

Fig 9: **(a)** Change in Load Demand **(b)** Wind Power Fluctuation **(c)** Variation in solar power irradiation

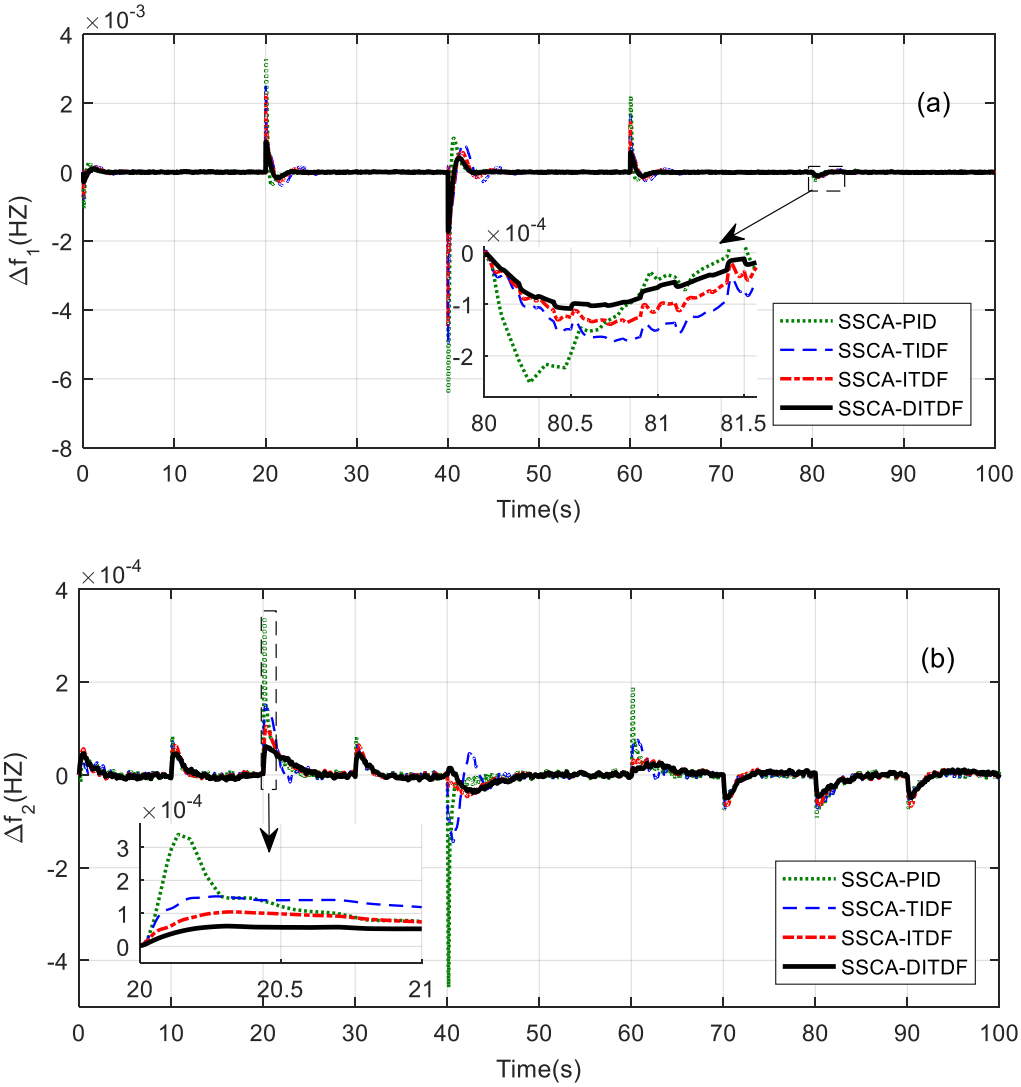

Fig. 10: Dynamic response of the MMG in **(a)** Area-1 and **(b)** Area-2 for case IV.

As a result, from the various critical analysis and simulations presented above in the section, it can be concluded that the proposed strategy outperforms its counterparts and provides a satisfactory stable and robust control.

5.3 Sensitivity Analysis

Sensitivity and robustness tests show that the suggested frequency controller for the MMG system is effective. Sensitivity study of the SSCA-DITDF controller refers to the impact of changes in the MMG system parameter on controller performance. In this section, the sensitive analysis is progressed with variation of time constant of different component of MMG system like WTG, PV, MT, BESS, EV, UC and DEG. To examine system performance under the suggested SSCA-DITDF controller, all of these parameters are regulated with a 40% reduction from their nominal values in this study. All of the responses were calculated without modifying the controller's optimal parameters, which were determined using the SSCA algorithm (see table 3). Table 8 specifies the Percentage variation in Performance Index J under during regulation of gain and time constant of different component of MMG. The figure 11 shows the sample response obtained under the case of WTG's component variation and compares it with nominal response. A thorough look at the results in Table 8 lucidly reveals the benefit of employing the DITDF controller in the MMG system for frequency regulation, when there is substantial variation in system parameters. Moreover. this shows that, in the context of unaltered controller parameters, broad system parameter adjustment has little impact on system performance. Furthermore, with extensive change of system parameters, critical study of all dynamic response suggests that to acquire the desired performance, there is no requirement of repeated retuning of the controller parameters.

Table 8: Percentage variation in Performance Index J under during regulation of time constant of different component of MMG.

Components	Variation of Gain and Time Constant of System Components	ITAE	%Change from Nominal Value
WTG	40% increase	0.8070	4.32%
	40% decrease	0.8067	4.28%
PV	40% increase	0.8533	9.51%
	40% decrease	0.7021	-9.97%
MT	40% increase	0.7124	-8.38%
	40% decrease	0.8386	7.73%
BESS	40% increase	0.7722	0.01%
	40% decrease	0.7723	0.02%
EV	40% increase	0.7706	-0.19%
	40% decrease	0.7735	0.18%
UC	40% increase	0.7217	-6.9%
	40% decrease	0.8340	7.4%
DEG	40% increase	0.7122	-8.4%
	40% decrease	0.8188	5.7%
M	40% increase	0.7726	0.06%
	40% decrease	0.7714	-0.09%
D	40% increase	0.7720	-0.01%
	40% decrease	0.7722	0.01%

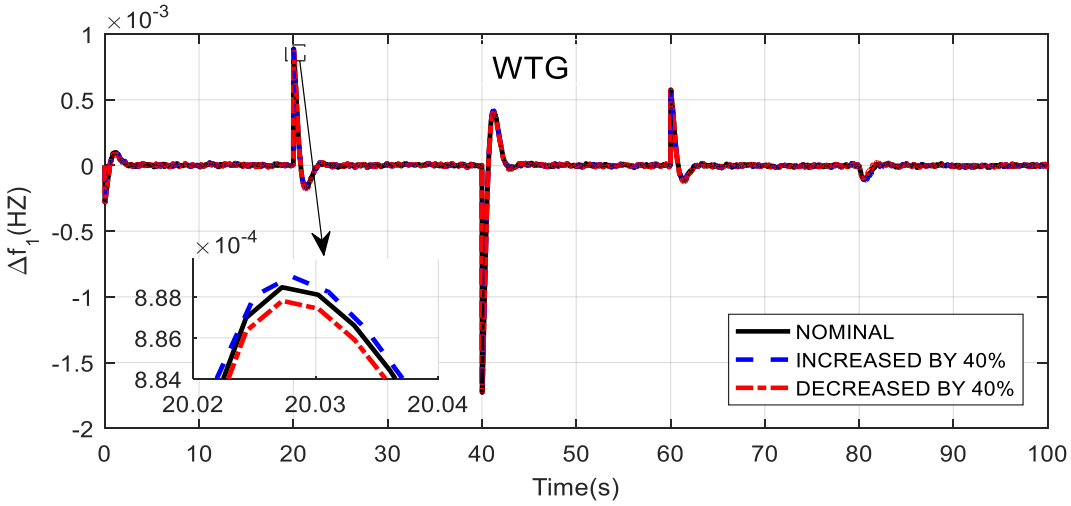

Fig. 11: Dynamic response under regulation of WTG

6. Conclusions

In this research work, a novel Double Integral Tilt Derivative with Filter (DITDF) controller is proposed for the LFC of the MMG system. Additionally, A novel variant of SCA, namely the Shrewd Sine–Cosine Algorithm (SSCA), is presented with an objective to eradicate the drawbacks of the SCA. The proposed SSCA is then tested using various benchmark functions to establish its efficacy over SCA, various popular algorithms (PSO, GA, GWO, GSA, SSA), and some recent modified SCA. It is noted that the SSCA outperforms the classical SCA in 19 out of the 20-benchmark function. Thus, suggesting its improvement in performance over the SCA. Moreover, while comparing some recent modifications of SCA, it provides the best result in 13 benchmark functions; for the remaining 7, it remains exceptionally competent, providing results close to the global minimum. The SSCA is then used for obtaining the optimal gains of the controllers used in the LFC of MMG. It is observed that the SSCA completely outperforms its competitors (GA/PSO/SCA) and provides the best controller performance during frequency regulation of MG, irrespective of the controller being used. To verify the suitability of the proposed SSCA- DITDF control scheme, the MMG is exposed to a variety of uncertain conditions by variation of load demand, solar power and wind power. It's fascinating to note that the suggested SSCA-DITDF controller entirely outperforms the likes of PID, TIDF and ITDF controller in terms of dynamic response. Even in the worst-case scenario, the SSCA-DITDF controller outperformed the PID, TIDF and ITDF controller by 38.78%, 32.12% and 18.99%. Finally, Sensitivity analysis is carried out to justify the robustness of the proposed SSCA optimized DITDF controller.

Appendix

DEG	$K_{DEG} = 1$ $T_{DEG} = 2$
PV	$K_{PV} = 1$ $T_{PV} = 1.8$
WTG	$K_{WTG} = 1$ $T_{WTG} = 1.5$
EV	$K_{EV} = 0.01$ $T_{EV} = 0.2$
BESS	$KB_{ESS} = -0.003$ $T_{BESS} = 0.1$
UC	$K_{UC} = -7$ $T_{UC} = 0.9$
MT	$K_{MT} = 1$ $T_{MT} = 2$

Abbreviations

MG	Microgrid
DER	Distributed Energy Resources
MMG	Multi-Microgrid
LFC	Load Frequency Control
NN	Neural Network
TID	Tilt-Integral-Derivative
PID	Proportional–Integral–Derivative
TIDF	Tilt-Integral-Derivative with Filter
ITDF	Integral Tilt Derivative with Filter Controller
DITDF	Double Integral Tilt Derivative with Filter Controller
GA	Genetic Algorithm
PSO	Particle Swarm Optimization
GSA	Gravitational Search Algorithm
GWO	Grey Wolf Optimizer
SSA	Slap Swarm Algorithm
DE	Differential Evolution
TLBO	Teaching Learning Based Optimization
SCA	Sine–Cosine Algorithm
EO	Equilibrium Optimizer
SSCA	Shrewd Sine–Cosine Algorithm
WTG	Wind Turbine Generator
PV	Photovoltaic System
UC	Ultra Capacitor
BESS	Battery Energy Storage System
DEG	Diesel Engine Generator
EV	Electric Vehicles
T/F	Transfer Function
ESS	Energy Storage System
SLP	Step Load Perturbation
ITAE	Integral Time Absolute Error

References

[1] Ackermann, T., Andersson, G., & Söder, L. (2001). Distributed generation: a definition. Electric Power Systems Research; 57(3), 195–204.

[2] Chowdhury, S., Chowdhury, S.P., & Crossley, P. (2009). Microgrids and Active Distribution Networks. The Institution of Engineering and Technology, London, United Kingdom; 1–320, doi: 10.1049/PBRN006E.

[3] Du, Y., Wang, Liu, G., Chen, X., Yuan, H., Wei Y., & Li, F. (2018). A cooperative game approach for coordinating multi-microgrid operation within distribution systems. Applied Energy, 222, 383-395. https://doi.org/10.1016/j.apenergy.2018.03.086.

[4] Vandoorn, T. L., Vasquez, J. C., De Kooning, J., Guerrero, J. M., & Vandevelde, L. (2013). Microgrids: Hierarchical control and an overview of the control and reserve management strategies. IEEE industrial electronics magazine, 7(4), 42-55.DOI: 10.1109/MIE.2013.2279306

[5] Kwasinski, A. (2011). Quantitative evaluation of DC microgrids availability: effects of system architecture and converter topology design choices. IEEE Trans Power Electron, 26(3), 835-851. doi: 10.1109/TPEL.2010.2102774.

[6] Sahoo, S.K., Sinha, A.K., & Kishore, N.K. (2018). Control techniques in AC, DC, and hybrid AC–DC microgrid: A review. IEEE Journal of Emerging and Selected Topics in Power Electronics, 6(2), 738–759.

[7] Li, C., Mao, Y., Zhou, J., Zhang, N. & An, X. (2017). Design of a fuzzy-PID controller for a nonlinear hydraulic turbine governing system by using a novel gravitational search algorithm based on Cauchy mutation and mass weighting. Applied Soft Computing, 52, 290-305.

[8] Gheisarnejad, M., & Khooban, M.H. (2019). Secondary load frequency control for multi-microgrids: HiL real-time simulation. Soft Comput 23, 5785–5798. https://doi.org/10.1007/s00500-018-3243-5

[9] Sahu, P.C., Mishra, S., Prusty, R.C., Panda, & S. (2018). Improved-salp swarm optimized type-II fuzzy controller in load frequency control of multi area islanded AC microgrid. Sustainable Energy, Grids and Networks, 16, 380-392. https://doi.org/10.1016/j.segan.2018.10.003.

[10] Pan, I., & Das, S. (2016). Fractional order fuzzy control of hybrid power system with renewable generation using chaotic PSO. ISA Transactions, 62, 19–29. https://doi.org/10.1016/j.isatra.2015.03.003

[11] Osinski, C., Villar Leandro, G., & da Costa Oliveira, G.H. (2019). Fuzzy PID Controller Design for LFC in Electric Power Systems. IEEE Latin America Transactions, 17(01), 147-154. doi: 10.1109/TLA.2019.8826706.

[12] Sahu, P.C., Prusty, R.C., & Panda, S. (2020) Frequency regulation of an electric vehicle-operated micro-grid under WOA-tuned fuzzy cascade controller. International Journal of Ambient Energy. DOI: 10.1080/01430750.2020.1783358

[13] Prakash, S., & Sinha, S.K. (2015). Neuro-Fuzzy Computational Technique to Control Load Frequency in Hydro-Thermal Interconnected Power System. J. Inst. Eng. India Ser. B 96, 273–282. https://doi.org/10.1007/s40031-014-0147-3

[14]. Yin, L., Yu, T., Yang, B., & Zhang, X. (2019). Adaptive deep dynamic programming for integrated frequency control of multi-area multi-microgrid systems. Neurocomputing, 344, 49-60.

[15] Das. S., & Panda. S. (2021). An optimized fractional order cascade controller for frequency regulation of power system with renewable energies and electric vehicles. Energy Syst. https://doi.org/10.1007/s12667-021-00461-9

[16] Gorripotu T.S., Samalla H., Jagan Mohana Rao C., Azar A.T., & Pelusi D. (2019) TLBO Algorithm Optimized Fractional-Order PID Controller for AGC of Interconnected Power System. In: Nayak J., Abraham A., Krishna B., Chandra Sekhar G., Das A. (eds) Soft Computing in Data Analytics. Advances in Intelligent Systems and Computing, vol 758. Springer, Singapore. https://doi.org/10.1007/978-981-13-0514-6_80.

[17] Das, S., Bhoi, S.K., Nayak, P.C., & Prusty, R.C. (2021). Slime Mould Algorithm Based Fractional Order Cascaded Controller for Frequency Control of 2-Area AC Microgrid. International Conference in Advances in Power, Signal, and Information Technology (APSIT), 1-6. doi: 10.1109/APSIT52773.2021.9641192.

[18] Nayak, P.C., Prusty, U.C., Prusty, R.C., & Panda, S. (2021). Imperialist competitive algorithm optimized cascade controller for load frequency control of multi-microgrid system. Energy Sources, Part A: Recovery, Utilization, and Environmental Effects, 380-392. DOI: 10.1080/15567036.2021.1897710 2018

[19] Pan, I., & Das, S. (2012). Intelligent fractional order systems and control: an introduction (Vol. 438). Springer.

[20] Lurie BJ. Three parameter tunable tilt-integral-derivative (TID) controller. U.S. Patent US5371670A, 1994.

[21] Sahu, R. K., Panda, S., Biswal, A., & Sekhar, G. C. (2016). Design and analysis of tilt integral derivative controller with filter for load frequency control of multi-area interconnected power systems. ISA transactions, 61, 251-264.

[22] Arya, Y. (2019). Impact of hydrogen aqua electrolyzer-fuel cell units on automatic generation control of power systems with a new optimal fuzzy TIDF-II controller. Renewable energy, 139, 468-482.

[23] Singh, K., Amir, M., Ahmad, F., & Khan, M. A. (2020). An integral tilt derivative control strategy for frequency control in multimicrogrid system. IEEE Systems Journal, 15(1), 1477-1488. doi: 10.1109/JSYST.2020.2991634

[24] Hakimuddin, N., Khosla, A., & Garg, J. K. (2020). Centralized and decentralized AGC schemes in 2-area interconnected power system considering multi source power plants in each area. Journal of King Saud University-Engineering Sciences, 32(2), 123-132.

[25] Safi, S. J., Tezcan, S. S., Eke, I., & Farhad, Z. (2018). Gravitational search algorithm (GSA) based pid controller design for two area multi-source power system load frequency control (LFC). Gazi University Journal of Science, 31(1), 139-153.

[26] Mirjalili, S., Mirjalili, S. M., & Lewis, A. (2014). Grey wolf optimizer. Advanced Engineering Software, 69, 46–61. https://doi.org/10.1016/j.advengsoft.2013.12.007.

[27] Mirjalili, S., Gandomi, A. H., Mirjalili, S. Z., Saremi, S., Faris, H., & Mirjalili, S. M. (2017). Salp Swarm Algorithm: A bio-inspired optimizer for engineering design problems. Advances in Engineering Software, 114, 163-191.

[28] Mirjalili, S. (2016). SCA: a sine cosine algorithm for solving optimization problems. Knowledge-based systems, 96, 120-133.

[29] Faramarzi, A., Heidarinejad, M., Stephens, B., & Mirjalili, S. (2020). Equilibrium optimizer: A novel optimization algorithm. Knowledge-Based Systems, 191, 105190.

[30] Hafez, A. I., Zawbaa, H. M., Emary, E., & Hassanien, A. E. (2016). Sine cosine optimization algorithm for feature selection. In 2016 international symposium on innovations in intelligent systems and applications (INISTA) (pp. 1-5). IEEE.

[31] Hamdan, S., Binkhatim, S., Jarndal, A., & Alsyouf, I. (2017). On the performance of artificial neural network with sine-cosine algorithm in forecasting electricity load demand. In 2017 International Conference on Electrical and Computing Technologies and Applications (ICECTA) (pp. 1-5). IEEE.

[32] Attia, A. F., El Sehiemy, R. A., & Hasanien, H. M. (2018). Optimal power flow solution in power systems using a novel Sine-Cosine algorithm. International Journal of Electrical Power & Energy Systems, 99, 331-343.

[33] Ramanaiah, M. L., & Reddy, M. D. (2017). Sine cosine algorithm for loss reduction in distribution system with unified power quality conditioner. i-Manager‘s Journal on Power Systems Engineering, 5(3), 10.

[34] Issa, M. (2021). Expeditious Covid-19 similarity measure tool based on consolidated SCA algorithm with mutation and opposition operators. Applied Soft Computing, 104, 107197.

[35] Gupta, S., & Deep, K. (2019). A hybrid self-adaptive sine cosine algorithm with opposition-based learning. Expert Systems with Applications, 119, 210-230.

[36] Gupta, S., & Deep, K. (2019). Improved sine cosine algorithm with crossover scheme for global optimization. Knowledge-Based Systems, 165, 374-406.

[37] Nayak, D. R., Dash, R., Majhi, B., & Wang, S. (2018). Combining extreme learning machine with modified sine cosine algorithm for detection of pathological brain. Computers & Electrical Engineering, 68, 366-380.

[38] Abd Elaziz, M., Oliva, D., & Xiong, S. (2017). An improved opposition-based sine cosine algorithm for global optimization. Expert Systems with Applications, 90, 484-500.

[39] Sahu, P. C., Prusty, R. C., & Panda, S. (2020). Approaching hybridized GWO-SCA based type-II fuzzy controller in AGC of diverse energy source multi area power system. Journal of King Saud University-Engineering Sciences, 32(3), 186-197.

[40] Nenavath, H., Jatoth, R. K., & Das, S. (2018). A synergy of the sine-cosine algorithm and particle swarm optimizer for improved global optimization and object tracking. Swarm and evolutionary computation, 43, 1-30.

[41] Liu, H., Hu, Z., Song, Y., Wang, J., & Xie, X. (2015). Vehicle-to-grid control for supplementary frequency regulation considering charging demands. IEEE Transactions on Power Systems, 30(6), 3110-3119.

[42] Zhu, X. (2009). Practical PID controller implementation and the theory behind. In 2009 Second International Conference on Intelligent Networks and Intelligent Systems (pp. 58-61). IEEE.

[43] Arya, Y. (2018). AGC of two-area electric power systems using optimized fuzzy PID with filter plus double integral controller. Journal of the Franklin Institute, 355(11), 4583-4617.

[44] Chen, S. C., & Kuo, C. Y. (2017). Design and implementation of double-integral sliding-mode controller for brushless direct current motor speed control. Advances in Mechanical Engineering, 9(11), 1687814017737724.

[45] Armghan, H., Yang, M., Armghan, A., & Ali, N. (2021). Double integral action based sliding mode controller design for the back-to-back converters in grid-connected hybrid wind-PV system. International Journal of Electrical Power & Energy Systems, 127, 106655.

Declarations

Availability of data and materials

All data generated or analyzed during this study are included in this published article.

Competing interests

The authors declare that they have no competing interests.

Funding

Not applicable

Authors' contributions

The first author has developed the models, designed the proposed novel controllers and algorithm, and analyzed the myriad results to delineate the effectiveness of the proposed strategies. The simplification is done by second author and he has provided all the technical guidance to complete the paper. Both the Authors have read and approved the Final Manuscript.

Acknowledgements

Not applicable

Shrewd Sine–Cosine Algorithm Based Double Integral Tilt Derivative Controller for Frequency Regulation of Multi Microgrid System

Satyajeet Das[1]* and Sidhartha Panda[2]

[1] Department of Electrical Engineering, Veer Surendra Sai University of Technology (VSSUT), Burla, 768018, Odisha, India, satyajeetburla@gmail.com.

[2] Department of Electrical Engineering, Veer Surendra Sai University of Technology (VSSUT), Burla, 768018, Odisha, India, prof.dr.spanda@gmail.com.

*Corresponding Author